SIMILARITY OF SEDIMENT TRANSPORT BY WATER AND AIR CURRENTS

BY

FRANCISCO CORONADO DEL AGUILA
SB, Ingeniero Civil, Universidad Nacional de Ingeniería
(1962)
SB, Ingeniero Agrícola, Universidad Agraria, La Molina
(1967)

Submitted in partial fulfillment
of the requirements for the degrees of

Master of Science, Civil Engineer

at the

Massachusetts Institute of Technology
(April, 1970)

Signature of Author . . . . . .
Department of Civil Engineering, (April 24, 1970)

Certified by. . . . .
Thesis Supervisor

Accepted by . . . . .
Chairman, Departmental Committee on Graduate Students

TO THE MEMORY OF MY FATHER

TO MY MOTHER

ABSTRACT

SIMILARITY OF SEDIMENT TRANSPORT BY WATER AND AIR CURRENTS

by

FRANCISCO CORONADO DEL AGUILA

Submitted to the Department of Civil Engineering on April 24, 1970 in partial fulfillment of the requirements for the Degrees of Master of Science and Civil Engineer.

The present investigation explores the possibility of using air currents to model the effects of water currents over a bed of sand, since the use of air flow could provide easier measurement of turbulence, easier handling of the sediments, less abrasion of machinery and more favorable laboratory working conditions for a number of problems.

The analysis comprised:

a) An analytical model for the bed and saltation load considering saltating sediment trajectories,

b) A two-dimensional mass conservation equation for the sediment in suspension,

c) Characteristic parameters that govern the sediment movement in a local scour problem.

Several modelling parameters were derived.

The experimental study was limited to verifying the applicability of the parameters for a local scour problem. Specifically, the experiments were designed to explore the action of a jet of water and of a jet of air issuing through a nozzle 0.25 inches in height and 6 inches in width over an initially flat bed of uniform granular sand. Three diameters of sand particles: 0.71, 0.59, 0.42 mm nominally were employed. Velocities were varied from 40 to 78 cm/sec in water and from 9 to 27 m/sec in air. Scour patterns were observed for 16 tests with different values of velocities and grain diameters under transient conditions up to the ultimate stable scour pattern.

The scour patterns for air and water jets could be represented by a single normalized shape which was within the range of the experiments, practically independent of time and of the ratio of jet velocity to the particle fall velocity. The validity of a single similarity parameter for the transfer of the scour pattern from the air model to the water prototype was confirmed.

Thesis Supervisor: Arthur T. Ippen

Title: Ford Professor of Engineering

ACKNOWLEDGEMENT

The author would like to thank The Agency for International Development, U.S. Department of State, The Agrarian University of Lima, Perú, and The Hydrodynamics Laboratory of the Department of Civil Engineering of M.I.T. for their economic support during my studies at M.I.T.

This study was supervised by Dr. Arthur T. Ippen, Ford Professor of Engineering. Dr. Ippen's helpful discussions and review of this work are greatly appreciated.

The author would also like to extend his thanks to Professor Lynn Gelhar for his kind advice during the design of the experimental equipment, to Mr. Roy Milley, machinist, and to everyone that in some way was helpful in the completion of this work.

Special thanks to Marilyn, my wife, for the support that she offered me, and for the fast and fine typing of this report.

TABLE OF CONTENTS

I. INTRODUCTION

Many people have been trying to explain the phenomena of sediment transport and have presented formulae to describe the rate of transport. Further, they have tried physical representations with laboratory model studies and mathematical models.

A theoretically correct description of the sediment transport has not yet been presented as a consequence of the number of variables involved in the process, and thus, an experimental study is still the most useful resource. This laboratory representation requires faithful adherence to similarity principles, at least, between the main forces driving the phenomena.

The most important problem for hydraulic engineers is that of particles, mostly of quartz, transported by a stream of water. The use of air as the fluid for a model representation of this phenomena has not been undertaken by hydraulic engineers, mainly because water is the basic element for a hydraulic laboratory and because it is easier to obtain sand of the same prototype, giving a very large difference in value between the sediment and the fluid densities.

Geologists and soil scientists have been using air currents in the laboratory but only to represent sediment transport by wind. So far, no one has tried to use air currents to model the flow of water currents, although they could provide easier measurements of turbulence, easier handling of the sediments, less abrasion of machinery, and more favorable laboratory working conditions for a number of problems.

An analysis of the modes of initiation of sediment movement, i.e., lifting, rolling, sliding, or some combination of these modes, leads to the conclusion that the Shields function (1) can give the critical conditions.

Since an equation describing the entire range of sediment movement is not available, the division of the sediment load into two groups, (a) sediment moving as bed load and in saltation, and (b) sediment moving in suspension and in wash load, is accepted in this study.

An analytical model for the bed and saltation load is presented with saltating sediment trajectories, considered as a limit for the first group: the sediment moving near the bed. The suspended sediment is studied using a two-dimensional mass conservation equation. The method of transforming the governing equations of motion to dimensionless form seems the most appropriate to find the parameters relating the forces governing the phenomena.

A heuristic approach is used for the local scour. The analyses are carried out without any initial restriction on the density of the fluid to be used in the model so that air currents may not be excluded.

The parameters proposed to model local scour are verified with a laboratory study where a jet of water submerged in water was the prototype and a jet of air submerged in air was the model. With the acceleration of gravity scale equal to one, the value of the normalized depth of scour scale is given by:

$$\left(\frac{\xi}{\ell}\right)_r = \frac{1}{L_r^{1/2}} \left(\frac{\rho_s - \rho_f}{\rho_s + k_2 \rho_f}\right)_r^{1/2}$$

It is suggested to carry additional laboratory studies and related prototype experiments to verify the generality of the parameters for local scour, and the significance of the parameters proposed to model bed and suspended load.

II. REVIEW OF PREVIOUS WORK

Even though air currents were not used so far to model natural streams of water transporting sediments, it is useful to present some of the work that has been done about similarity studies in either mode of sediment transport. Studies using water to model water currents will be presented first, followed by studies using air currents.

General treatments of the theory of similarity can be found in many books, see for instance references (3) to (7). References (8) to (10) deal specifically with hydraulic models.

The laboratory studies of streams of water can be divided into the so-called fixed and movable bed models. Both types of representation can be either distorted or undistorted in the scales.

Fixed bed models are useful to study situations in which actual changes in bed configuration are not critical. Foster (11) presents a good description of fixed bed models and gives several examples of laboratory studies. The scales are chosen following the Froude law and a formula to compute the roughness factor. It is possible to study the sediment transport behavior around or in hydraulic structures, i.e. intakes and sandtraps, adding the sediment to the fixed bed, as it was used in the studies described in references (12) and (13).

Movable bed models serve to investigate problems involving scour, transportation, and deposition of sediments. Examples can be found in references (7) and (8). The scales for the laboratory representation are in general obtained by transforming to dimensionless form any of the

empirical or semi-empirical sediment load rate equations, or from parameters obtained through dimensional analysis.

Little can be concluded about the advantage of using one specific bed load formula over another since each one is the result of hypotheses, assumptions or some experimental results, and consequently all formulae have limitations, as can be learned by reviewing references (14) to (24). The lack of extensive conformity studies between models and prototypes makes the selection of a specific formula more difficult.

Presenting a purely empirical formula Blench (19), (25) gives a summary of the so-called regime theory. According to this "theory", channels in regime are those which, carrying a sediment load, are capable of adjusting their solid boundaries to an equilibrium profile. Its basic results are three relations involving the average width b, the depth y_o and channel slope S_o, with the discharge Q in the form:

$$b,\ y_o,\ S_o = kQ^j \qquad (2.1)$$

where k and j are dimensional constants. As indicated by Einstein (26), with this theory it is impossible to obtain scales for the sediment size and sediment discharge. Of all the semi-empirical bed load equations, those by Meyer-Peter, Müller (17) and Einstein (18) are the most commonly used.

The Einstein bed load functions (18) have been more extensively employed in the United States and in many parts of the world. It is one of the most important attempts to rationalize the calculations of the sediment discharge using basic concepts of fluid mechanics like laminar

sublayer, turbulent fluctuations as expressed in some way in his probabilistic analysis for the sediment movement, and some sediment characteristics like the particle shielding effects. Colby and Hembree (27) presented a modification of the Einstein bed load computations, given also in reference (28). Vanoni and Brooks (29) present a simpler procedure to calculate the hydraulic radius using a working chart. They questioned some assumptions of the Einstein theory, like the height limit of the bed load and the use of a unique value for the Von Karmán constant, especially with various bed forms. Since until now there has not been any more rational analysis as to how his parameters vary, Einstein's assumptions remain acceptable.

Einstein and Chien (2) proposed several criteria to calculate the scales for a movable bed model, namely: a friction criterion using a generalized Manning equation, a Froude criterion, a laminar sublayer criterion, a sediment transport and a zero sediment load criterion. The sediment transport criterion uses the Einstein intensity transport parameter Φ_*

$$\Phi_* = \frac{i_B}{i_b} \frac{q_s}{g(\rho_s - \rho_f)} \left(\frac{\rho_f}{\rho_s - \rho_f} \right)^{1/2} \left(\frac{1}{gd^3} \right)^{1/2} \qquad (2.2)$$

for different fluids in model and prototype but for the same mixture of grain sizes, it can be written as:

$$\left[q_s (\rho_s - \rho_f)^{-3/2} \rho_f^{1/2} d^{-3/2} \right]_r = 1 \qquad (2.3)$$

where q_s is the sediment bed load rate, ρ_s and ρ_f are the sediment and fluid density respectively, d is the characteristic sediment diameter, and the subindex r denotes the ratio between the values of model and prototype. The zero sediment load criterion uses Einstein's intensity shear parameter Ψ_*, that is, a Shields parameter (1) with some corrections, and, taking the ratio between the corrections for model and prototype equal to one, obtain the Shields parameter ratio, as will be defined in the section on initiation of sediment movement. Einstein and Chien also mention the possibility of having up to seven distortions.

Bogardi (29) considers the Einstein-Chien parameters satisfactory, but as a complement proposes another parameter, his channel stability factor that is a sort of shear Froude number.

Yalin (20) presents an expression for bed load rate of transport assuming a saltation model, in which the particles move on a ballistic trajectory. His model of a saltation pattern as a limit for the sediment moving as bed load seems reasonable.

The study by Rouse (31) employing dimensional analysis will be mentioned next. He gives the relationships for bed load movement, sediment transport in suspension, and local scour, including the sediment sorting characterized by the standard deviation σ_s of the particles, or the particles fall velocity variation characterized by the standard deviation σ_w of the fall velocity. He arrives at four dimensionless parameters containing six variables when a dimensional analysis allows only three independent groups. For bed load he considers the action of shear stress τ_o sediment and fluid specific weight ratio γ_s/γ_f, the degree of immersion of particles of diameter d, inside the laminar sublayer thickness δ,

in the form

$$\frac{\tau_o}{\gamma_f d} = f\left(\frac{\gamma_s}{\gamma_f}, \frac{d}{\delta}, \sigma_s\right) \tag{2.4}$$

In the case of movement of sediment in suspension, he proposes the concentration C_a at a level a as a function of the relative height a/y_o, where y_o is the local flow depth, and the ratio between shear and fall velocity

$$C_a = f\left(\frac{a}{y_o}, \frac{u_*}{w}, \sigma_w\right) \tag{2.5}$$

For local scour, he writes a function for the geometrical characteristics of the scour depth ζ in terms of the characteristic length ℓ of the scour, depending on the ratio between the flow velocity U and particle fall velocity w and a kinematic relation wt/ℓ (taking into account the transient conditions).

$$\frac{\zeta}{\ell} = \phi\left(\frac{wt}{\ell}, \frac{U}{w}, \sigma_w\right) \tag{2.6}$$

Yalin (32) proposed 4 dimensionless groups: a Reynolds number, du_*/ν, the relative height of the sediment size y_o/d, a parameter similar to the Shields function (but without taking into account the buoyant effect of the volume of fluid displaced by the sediments) $\rho_f u_*^2/g\rho_s d$ the density ratio ρ_s/ρ_f.

Field (33), using dimensional analysis and an analysis of a particle in unsteady movement, suggests a length scale, $(\rho_s/\rho_f + k_2)d$, and a time scale $(\rho_s/\rho_f + k_2)[d/g(\rho_s/\rho_f - 1)]^{1/2}$. Experimenting with a horizontal

submerged jet of water he presents a plot of the maximum length of scour and time normalized with respect to his own scales. He concludes that his scale ratios give better correlation for various sediment to fluid density ratios, although his plot of his data against Rouse (31) parameters shows a more defined trend in this latter case.

Barr and Herbertson (34) introduced the concept of dynamic velocity defined, by the authors, as being proportional to that velocity that would be attained if a representative element were to be acted on by an active force, as it affects the element in the system through a representative distance. Clearly, this concept represents the combination of dimensional magnitudes with a dimension of velocity. It is not clear, however, why they have to combine these dimensional ratios to obtain relations with dimensions of length, and then, form the ratio of these new groups to obtain the dimensionless parameters. It seems that this procedure adds unnecessary difficulties in the analysis of a phenomena, and makes loose the physical meaning of the dimensionless parameters.

Using mathematical models, Gradowczyk and Folguera (35) studied the scour in open channels, using the energy equation for unsteady flow, a friction factor formula, and a sediment transport equation. The use of a sediment transport formula introduces some coefficients which the authors suggest obtaining from physical experiments.

In the case of sediment movement by air currents, the laboratory studies have been reduced to find expressions for the rate of sediment transport.

From wind tunnel studies, Bagnold (36), Zingg (37), and Chepil (38) present a relation of the form

$$q_s = \frac{e(d/d_o)^p \rho_f}{g(\tau/\rho_f)^{3/2}} \qquad (2.7)$$

where e is a dimensional coefficient varying with the gradation of the sediment, the proportion of fine dust, roughness of the field, and amount of moisture in the soil; d/d_o is the ratio of the sand mean size d to the mean size d_o of a standard sand taken as 0.25 mm; p is an exponent equal to 1/2 in Bagnold's results and 3/4 in Zingg's studies.

Kawamura (22), assuming a division in the shear stress on the bed surface τ in the form $\tau = \tau_s + \tau_w$ where τ_s is an impact shear stress, and τ_w is a horizontal shear stress, writes for q_s in lb/ft-sec.

$$q_s = K\rho_s(u_* + u_{*c})^2(u_* - u_{*c}) \qquad (2.8)$$

where K is a dimensionless coefficient, u_* and u_{*c} are the shear velocity and the threshold shear velocity respectively. He makes use of the Stokes law for the fall velocity of spherical particles even when he himself recognizes that, in general, the characteristics of the fall are far from being laminar.

Kadib (23) makes an attempt to relate the sediment transport by air and water, using the Einstein procedure for bed load.

It is clear that the different approaches used to obtain the amount of sediment transported by water and air currents have to give differences among the formulae proposed to determine the rate of sediment discharge, making impossible the selection of one specific formula for a laboratory representation of the action of water currents on a bed of sediments

using air currents. In this situation, it seems advisable to analyze the sediment movement without specifying the nature of the fluid and sediment in order to find parameters that could be used in a model study.

III. THEORETICAL ANALYSIS

3.1. Initiation of movement

For a fluid flowing over a loose bed, there exists near the bed a mean velocity profile $u = u(y)$ and superimposed turbulent velocity fluctuations. The fluid force exerted on the sediments may be resolved into two components, one parallel to the direction of the mean flow, called the drag, and the other normal to the first, called the lift.

For noncohesive sediments such as sands and gravels, the forces resisting motion are caused mainly by the weight of the particles diminished by the buoyancy effect of the fluid.

The grains of sediments begin their movements in various modes: by lifting, by rolling, by sliding or by a combination of these forms such as rolling and sliding.

Considering lifting as the first mode of sediment movement, it is worth mentioning the work of Jeffreys (39) who explains that the pressure distribution on a solid particle resting on the bottom of a stream produces a lifting force on this particle.

In the following derivation only the lift force will be considered. The drag force will be considered as not having much effect at the beginning of motion.

If we call ϕ the bed slope, θ the angle of internal friction for the sediments, in static loose conditions equal to the angle of repose of the material, we can write:

$$L = F_r + W \cos \phi \qquad (3.1.1)$$

where: L is the lift force and F_r is the component of the resultant frictional force between the particles. The lift force is usually expressed as:

$$L = C_L A \rho_f \frac{u^2}{2} \tag{3.1.2}$$

wherein C_L is a lift coefficient which is a function of a shape factor k_1 and of the sediment shear Reynolds number, $u_* d/\nu$; A is the projected section of the grain normal to the lift force, and equal to $k_1 d^2/4$.

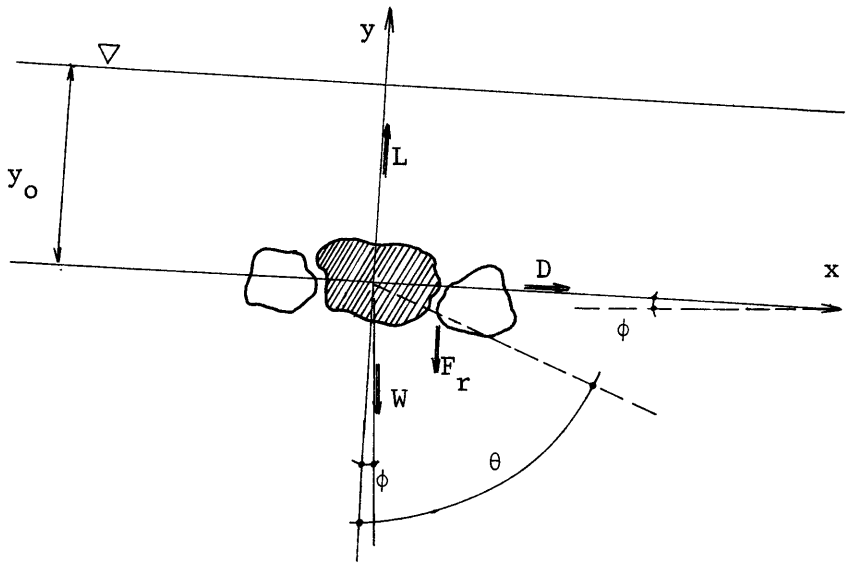

Fig. 1. Schematic diagram of forces acting on a grain

For air and water the velocity distribution can be written:

for smooth boundary: $\frac{u}{u_*} = 5.75 \log \frac{y u_*}{\nu} + 5.5$

for rough boundary: $\frac{u}{u_*} = 5.75 \log \frac{y}{k_e} + 8.5$

writing $y = \eta d$ and assuming the height of roughness k_e proportional to the sediment diameter d, the height y will be proportional to k_e:

$$\frac{yu_*}{\nu} \propto \frac{k_e\, u_*}{\nu} \propto \frac{k_e}{\delta'} \quad , \quad \text{where } \delta' = \frac{11.6\nu}{u_*}$$

and the velocity distribution can be written as:

$$\frac{u}{u_*} = 5.75 \log \eta + f\left(\frac{u_* d}{\nu}\right)$$

where the values 5.5 and 8.5 have been presented as a function of $u_* d/\nu$, in a general form we can write:

$$u = u_*\, f_1\left(\eta, \frac{u_* d}{\nu}\right) \qquad (3.1.3)$$

Bagnold (21), Kadib (23) and Chiu (24) have utilized essentially the same formula:

$$u = 5.75\, u_*\, \log \frac{y}{k_e} + u_c$$

where u_c is a so-called threshold velocity which must be a function of $u_* d/\nu$. Hence this velocity distribution is identical to equation (3.1.3).

The lift force can then be presented in the form

$$L = k_1 \frac{\pi d^2}{4} \rho_f \frac{u_*^2}{2} f_1\left(\eta, \frac{u_* d}{\nu}\right) C_L\left(\text{s.f.}, \frac{u_* d}{\nu}\right),$$

or

$$L = k_1 \frac{\pi d^2}{8} (\rho_f\, u_*^2)\, f_2\left(\eta, \text{s.f.}, \frac{u_* d}{\nu}\right),$$

recognizing that the bed shear stress $\tau_o = \rho_f\, u_*^2$,

$$L = \frac{k_1 \pi}{8} \tau_o d^2 f_2 \left(\eta, \text{ s.f.}, \frac{u_* d}{\nu}\right) \qquad (3.1.4)$$

From the equilibrium of forces in the y direction, as shown in Fig. 1, the force F_r, the resultant friction force, is

$$F_r = [D + W \sin \phi] \tan \theta$$

Neglecting the particle horizontal drag D,

$$F_r = W \sin \phi \tan \theta \qquad (3.1.5)$$

the submerged weight W can be written as:

$$W = \frac{\pi d^3}{6} (\rho_s - \rho_f) g \cos \phi \qquad (3.1.6)$$

replacing (3.1.4), (3.1.5) and (3.1.6) in equation (3.1.1), we obtain

$$\frac{\tau_o}{gd(\rho_s - \rho_f)} = \frac{4}{3} \frac{1}{k_1} \frac{\cos \phi \ (\sin \phi \tan \theta + 1)}{f_2\left(\eta, \text{ s.f.}, \frac{u_* d}{\nu}\right)} \qquad (3.1.7)$$

In most cases the slope of the bottom is small, therefore the value of sin ϕ is approximately zero and cos ϕ is near unity. In addition, for nearly spherical particles the shape factor is also nearly unity. Hence for y approximately equal to d, equation (3.1.7) reduces to the Shields function β_c (1),

$$\beta_c = \frac{\tau_c}{gd(\rho_s - \rho_f)} = f\left(\frac{u_* d}{\nu}\right) \qquad (3.1.8)$$

In water, β_c has a value of approximately 0.056, as is seen from Fig. 2. In air, Bagnold (21) obtained, in the case of movement of a few particles, an approximate value of $\beta_c = 0.056$ as confirmed by Chepil (38). With an appreciable number of particles moving, the impact of the first few particles in movement over the grains still on the bed exercises an additional force on the particles, making necessary a lower value of the bed shear stress due to the flow, to initiate the movement. In this case the critical Shields function has an approximate value of 0.0064.

Considering rolling of particles as initiation of sediment movement, the Committee on Preparation of the Sediment Manual of the ASCE (41) includes the lift effects in the drag force, considered parallel to the bed, and taking moments with respect to the particle support points expresses a critical shear stress in the form:

$$\frac{\tau_c}{gd(\rho_s - \rho_f)} = k \cos \phi \ (\tan \theta - \tan \phi) \qquad (3.1.9)$$

where k is a coefficient which is a function of the shape of the particle, the structure of the soil, the angle of internal friction of the particles θ, and the bed slope ϕ. For horizontal or nearly horizontal beds, (3.1.9) reduces to:

$$\frac{\tau_c}{gd(\rho_s - \rho_f)} = c \tan \theta \qquad (3.1.10)$$

This formula was presented earlier by White (42), assuming negligible lift.

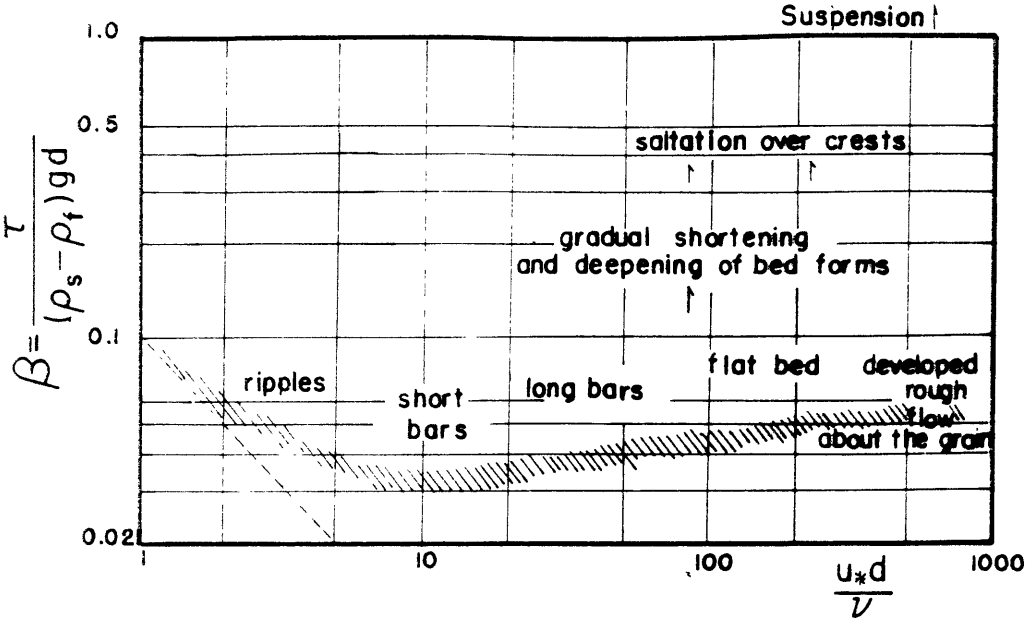

Fig. 2 Initiation of movement conditions. Shields (1)

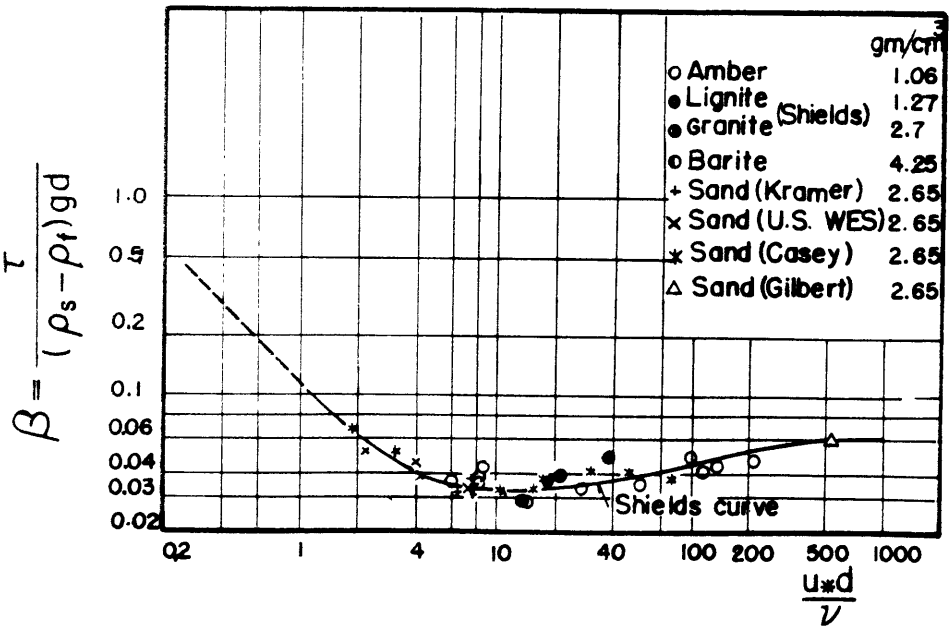

Fig. 3 Beginning of bed load movement. Vanoni (44)

Considering the sliding of particles as the first mode of movement, Carstens, Neilson and Altinbilek (43) write:

$$\frac{\tau_c}{gd(\rho_s - \rho_f)} = \frac{\tan\theta \cos\phi + \sin\phi}{1 + \tan\theta} \frac{k}{C'_D} \qquad (3.1.11)$$

where k is a constant and C'_D is the drag coefficient for a freely falling particle. Using a velocity distribution, as described for the lifting process $u = u_* f_1 \left(\frac{u_* d}{\nu}\right)$, a horizontal or nearly horizontal bed, and with k and C'_D functions of the shear Reynolds number, it is possible to obtain:

$$\frac{\tau_c}{gd(\rho_s - \rho_f)} = \frac{\tan\theta}{1 + \tan\theta} f\left(\frac{u_* d}{\nu}\right) \qquad (3.1.12)$$

representing a correction to the Shields function value for the different angles of internal friction of the particles, i.e. with $\theta = 30°$, there is a reduction of approximately 60% in the Shields function value.

The variation of the critical value for the initiation of movement as presented by Shields (Fig. 2) has been discussed at length and attributed to many factors: the bed gradation, soil structure that could be described by a shape factor, angle of internal friction, bed slope, and the density difference between fluid and sediment, which represents different inertial responses to turbulent fluctuations. Vanoni (44), following an earlier plot by Rouse, has drawn a curve over the Shields, Kramer, Gilbert and the USWES data, Fig. 3.

Ippen and Verma (45), in the case where a few particles moved over a rough rigid bed, having a length roughness k_e smaller than the particles

diameter d, proposed an empirical correction to the Shields function in the form:

$$\frac{\tau_c}{gd(\rho_s - \rho_f)} = \frac{\rho_f}{\rho_s} \frac{k_e}{1.5} f \left(\frac{u_* d}{\nu} \right) \tag{3.1.13}$$

Ward (46), in the cases of rolling and sliding, rolling without sliding, or sliding without rolling, writes the equilibrium equations for the tangential direction indicated by the angle of repose, normal direction, and the momentum about the center of mass of the particle, considering the resultant forces of drag and lift, acceleration of the particles in the direction indicated by the angle of repose, zero angular velocity. After solving the equations two by two, Ward obtains results of the form:

$$\frac{\tau_c}{gd(\rho_s - \rho_f)} = k_1 \{1 + \left(\frac{\rho_s}{\rho_s - \rho_f} \right) k_2\} \tag{3.1.14}$$

where k_1 and k_2 are functions of the shear Reynolds number and become constant for fully turbulent flow. His results can be written as a functional relationship of the form:

$$\frac{\tau_c}{gd(\rho_s - \rho_f)} = f \left(\frac{\rho_s}{\rho_s - \rho_f}, \frac{u_* d}{\nu} \right) \tag{3.1.15}$$

A three-dimensional representation considering a third axis for density ratios gives a surface of critical values for the Shields function. Ward presents his own experimental data plotted in a Shields representation showing noticeable differences with the Shields curve, as represented by Vanoni (44). Using as the ordinate the values of the Shields parameter

β_c divided by the factor $[1 + 1.25(\rho_s/\rho_s - \rho_f)]$, he obtains a reduction of scatter for his data; however, he does not present the reduced value of Shields, Kramer, etc. Plotting these data, appreciable scatter of the later experimental values is observed.

From the preceding presentation it is possible to conclude generally that the Shields function can be used as the parameter for the initiation of movement, regardless of the mode of initiation of sediment movement.

3.2. Delimitation of the modes of sediment movement

It has been observed in many laboratory studies that sediment transport has several distinctive modes. When velocities are low enough, the transport occurs primarily by rolling and sliding along the bed surface. With higher velocities particles are lifted a considerable distance above this surface but return to the surface within a relatively short distance. This process has been termed saltation. When the turbulent velocities are increased further, particles are transferred to still higher levels in the fluid and remain in the main body of the turbulent stream for extensive periods of time or indefinitely. It is said that this mode of transport represents suspension, i.e., statistically speaking, a certain amount is carried at the higher levels of the stream at average concentrations. These concentrations are a function of the turbulent mechanism and of the settling velocity. Referring to Figs. 2 and 3, these three modes of transportation may be approximately characterized by various values of the parameter β as derived in the preceding section.

The average values of β are:

1. $0(10^{-2}) < \beta < 1$ primarily movement as bed and saltation load

2. $\beta \geq 1$ primarily movement as suspension and wash load.

Sutherland (47) remarks that suspension occurs when the upward fluid velocity exceeds the grain fall velocity before the grain settles back to the bed. Bagnold (48) expresses a limiting function B_s for the initiation of suspension in the form:

$$B_s = 0.64 \frac{w^2}{gd} \frac{\rho_f}{\rho_s - \rho_f} \tag{3.2.1}$$

that can be related to the Shields function β in the form:

$$B_s = 0.64 \frac{w^2}{gd} \frac{\rho_f}{\rho_s - \rho_f} \frac{u_*^2}{u_*^2} = 0.64 \frac{w^2}{u_*^2} \beta \tag{3.2.2}$$

Considering the equilibrium between the drag force and the sediment submerged weight the mean fall velocity w can be written in the form

$$w \propto \sqrt{(\rho_s - \rho_f)d}$$

instead of equation (3.2.2) we could have

$$B_s = \text{constant}$$

For grains of quartz in water equation (3.2.1) gives

$$B_s = 0.4 \left(\frac{w^2}{gd} \right) \tag{3.2.3}$$

for grains of quartz in air, it is possible to write:

$$B_s = 0.0003 \frac{w^2}{gd} \qquad (3.2.4)$$

From Bagnold's plot in Fig. 4, we could conclude that particles smaller than 0.1 mm can move only in suspension, but this limiting diameter is open to question, since for low enough velocities it is possible to have even these particles, slipping, rolling, or saltating. According to the same Fig. 4, the suspension criterion of β=1 could be valid only for grain sizes larger than 1 mm, but if instead of considering the grain diameter we consider the grain Reynolds number, this limiting size corresponds to highly turbulent flows, which is generally the case for natural streams of water. Thus, the Shields function value β=1 can be accepted as a lower limit for sediment moving in suspension.

3.3. Saltation and bed load movement

3.3.1. General model

Since the thickness of the layer of saltating cohesionless particles in water has been accepted to be between 2 or 3 mean particle diameters (18), and since the motion of the same kind of particles in air is mostly in saltation (21), it may be assumed here that the bed load movement can be considered as a characteristic saltation pattern. Hence, the forces acting on a grain in a two-dimensional motion should be studied as for the case of movement in water by Yalin (20), and for movement in air by Bagnold (21) and Owens (49).

A two-dimensional analysis considering the equilibrium of a particle as shown in Fig. 5 follows.

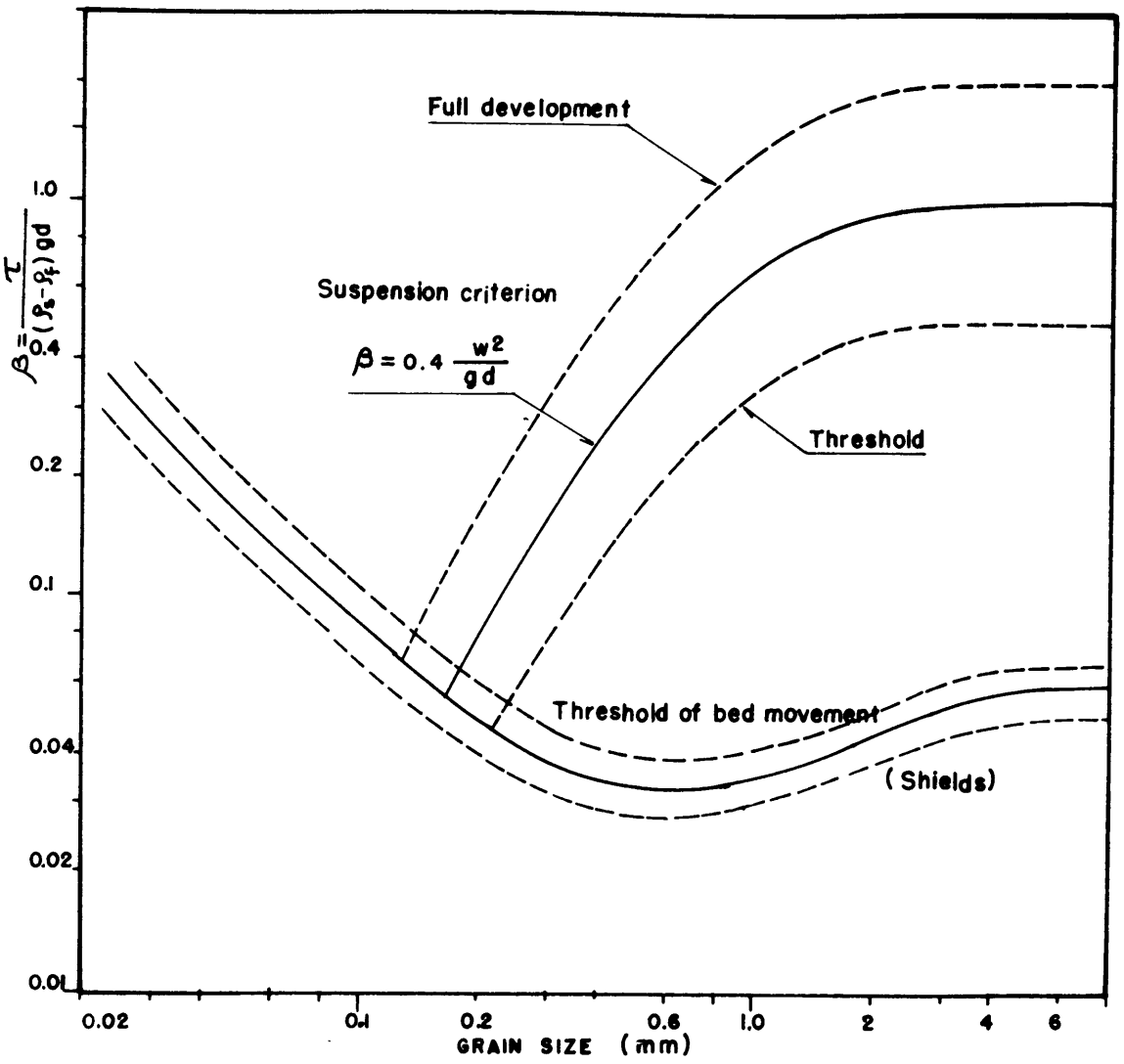

Fig 4 Suspension criterion. Bagnold (48)

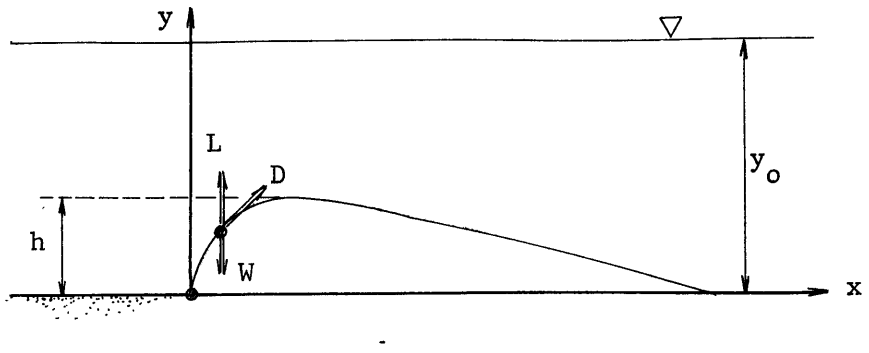

Fig. 5. Characteristic sediment saltation pattern

1. Sediment motion in the y direction.

The equilibrium of a particle at any time and position can be described by the equation:

$$m \frac{d^2y}{dt^2} = L - D(y) - W \qquad (3.3.1)$$

At the bed the lift force L_o can be written, as obtained in section 2.1, in the form:

$$L_o = k_1 \frac{\pi}{8} \rho_f u_*^2 d^2 f_2(\eta, \text{s.f.}, \frac{u_* d}{\nu})$$

Defining a critical lift force L_{oc} equal to the submerged weight of the particle, this particle begins to move when:

$$L_{oc} = W = k_1 \frac{\pi}{8} \rho_f u_{*c}^2 d^2 f_2(\eta, \text{s.f.}, \frac{u_* d}{\nu})$$

It is then possible to write the general ratio for the lift force on the bed to submerged weight as:

$$\frac{L_o}{W} = \frac{L_o}{L_{oc}} = \frac{f_2(\eta,\ s.f.,\ u_* d/\nu)}{f_2(\eta,\ s.f.,\ u_{*c} d/\nu)} \frac{u_*^2}{u_{*c}^2}$$

The functions f_2 can be considered equal since, in the region of sediment motion, the particles pass from a thin transitional zone to a turbulent zone where the function f_2 varies only slightly with the Reynolds number, thus:

$$\frac{L_o}{W} = \frac{u_*^2}{u_{*c}^2}$$

At a level y over the bottom the ratio of lift force to submerged weight can be written

$$\frac{L}{W} = \frac{L_o}{W} f\left(\frac{y}{d}\right) = \frac{u_*^2}{u_{*c}^2} f\left(\frac{y}{d}\right) \qquad (3.3.2)$$

In order to define the function f(y/d) it has to be remembered that the lift force L has to be equal to the maximum lift force L_o at the bottom, and equal to zero at the maximum height of the saltation path.

$$f(y/d) = 1 \qquad \text{at} \quad y/d = 0,$$
$$f(y/d) = 0 \qquad y/d \to \frac{y_{max}}{d}$$

for simplicity a function of the form

$$f\left(\frac{y}{d}\right) = 1 - \alpha \frac{y}{d}$$

may be introduced, where α has to be less than one, has to be determined experimentally and is of an order of magnitude of $1/y_o$.

D(y), the vertical projection of the drag force, can be written as a function of the submerged weight. Considering the s direction, tangent to the trajectory of the particle, and the velocity ds/dt, one may write

$$D(s) = W \frac{ds/dt}{w}$$

Besides, the projection D(y), see Fig. 6, is equal to

$$D(y) = D(s) \frac{dy/dt}{ds/dt}$$

therefore:

$$D(y) = W \frac{dy/dt}{w} \qquad (3.3.3)$$

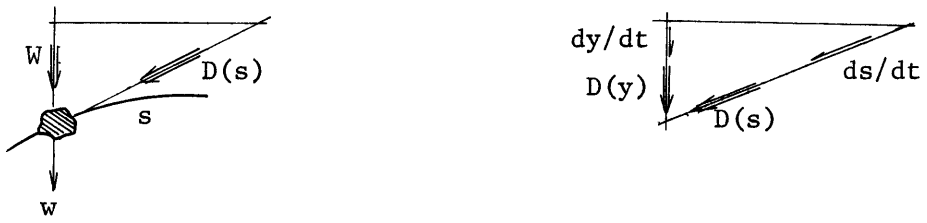

Fig. 6. Vertical drag force D(y) determination

W, the submerged weight can be expressed in the form:

$$W = \frac{\pi d^3}{6} (\rho_s - \rho_f)g \qquad (3.3.4)$$

m, the virtual mass is equal to:

$$m = \frac{\pi d^3}{6} (\rho_s + k_2 \rho_f) \tag{3.3.5}$$

where k_2 is the added mass coefficient.

Equation (3.3.1) can be written, after dividing by W, in the form

$$\frac{m}{W} \frac{d^2y}{dt^2} = \frac{L}{W} - \frac{D(y)}{W} - 1 \tag{3.3.6}$$

Replacing the expressions for the virtual mass, submerged weight, lift and vertical projection of the drag force:

$$\frac{1}{g} \left(\frac{\rho_s + k_2 \rho_f}{\rho_s - \rho_f} \right) \frac{d^2y}{dt^2} = \frac{u_*^2}{u_{*c}^2} \left(1 - \alpha \frac{y}{d}\right) - \frac{1}{w} \frac{dy}{dt} - 1 \tag{3.3.7}$$

Setting:

$$\left(\frac{\rho_s - \rho_f}{\rho_s + k_2 \rho_f} \right) g = G \quad , \quad \text{and}$$

$$\frac{u_*^2}{u_{*c}^2} = M$$

equation (2.3.7) can be written:

$$\frac{d^2y}{dt^2} + \frac{G}{w} \frac{dy}{dt} + \alpha \frac{MG}{d} y = G(M - 1) \tag{3.3.8}$$

the initial condition is: at t=0, y=0, dy/dt = 0

and the final condition: at t=T, duration of the saltation, y=0

The homogeneous part of equation (3.3.8) has 3 possibilities, setting

$$\left(\frac{G}{w}\right)^2 - \frac{4\alpha MG}{d} = k^2 \quad ,$$

a) $k > 0$

$$y_h = c_1 e^{\frac{-\frac{G}{w} + k}{2} t} + c_2 e^{-\frac{\frac{G}{w} - k}{2} t}$$

b) $k = 0$

$$y_h = (c_1 + c_2 t)\, e^{-\frac{G}{2w} t}$$

c) $k < 0$

$$y_h = e^{-\frac{G}{2w} t} (c_1 \cos kt + c_2 \sin kt)$$

the particular solution is

$$y_p = \frac{M - 1}{M} \frac{d}{\alpha}$$

Working with the first possibility, (a), applying first the final condition, $c_2 = 0$; with the initial condition,

$$y = \frac{M - 1}{M} \frac{d}{\alpha} \left(1 - e^{\frac{\frac{G}{w} - k}{2} t}\right)$$

where $\frac{G}{w}$ has to be larger than k in order to have solutions. Besides, we must have for the maximum height of saltation zero velocity, thus:

$$\frac{dy}{dt} = \frac{M - 1}{M} \frac{d}{\alpha} \left(- \frac{\frac{G}{w} - k}{2}\right) e^{- \frac{\frac{G}{w} - k}{2} t}$$

at the maximum height, $t \neq 0$ and $dy/dt = 0$, so, the only possibility is $G/w = k$, which is incompatible with the condition that a solution must exist.

Working with the second possibility, (b), with the initial condition $y = 0$ at $t = 0$

$$c_1 = - \frac{M - 1}{M} \frac{d}{\alpha} ,$$

and

$$y = \left(- \frac{M - 1}{M} \frac{d}{\alpha} + c_2 t\right) e^{- \frac{G}{2w} t} + \frac{M - 1}{M} \frac{d}{\alpha} ,$$

now:

$$\frac{dy}{dt} = \left(- \frac{G}{2w}\right) \left(- \frac{M - 1}{M} \frac{d}{\alpha} + c_2 t\right) e^{- \frac{G}{2w} t} + c_2 e^{- \frac{G}{2w} t}$$

with $dy/dt = 0$ at $t = 0$

$$c_2 = - \frac{G}{2w} \frac{M - 1}{M} \frac{d}{\alpha} ,$$

so:

$$y = \frac{M - 1}{M} \frac{d}{\alpha} \left[1 - \left(1 + \frac{G}{2w} t\right) e^{- \frac{G}{2w} t}\right]$$

This solution gives at $t = T \neq 0$, $y \neq 0$ and has to be rejected.

Working with the last possibility, c, with the initial condition $y = 0$ at $t = 0$,

$$c_1 = - \frac{M - 1}{M} \frac{d}{\alpha}$$

thus:

$$y = e^{- \frac{G}{2w} t} \left(- \frac{M - 1}{M} \frac{d}{\alpha} \cos kt + c_2 \sin kt\right) + \frac{M - 1}{M} \frac{d}{\alpha} ,$$

$$\frac{dy}{dt} = e^{- \frac{G}{2w} t} \left(k \frac{M - 1}{M} \frac{d}{\alpha} \sin kt + c_2 k \cos kt\right) -$$

$$\frac{G}{2w} e^{- \frac{G}{2w} t} \left(- \frac{M - 1}{M} \frac{d}{\alpha} \cos kt + c_2 \sin kt\right)$$

but at $t = 0$; $dy/dt = 0$, then

$$c_2 = - \frac{1}{k} \frac{G}{2w} \frac{M - 1}{M} \frac{d}{\alpha} ,$$

and:

$$y = \frac{M - 1}{M} \frac{d}{\alpha} \left[1 - \left(\cos kt + \frac{1}{k} \sin kt\right) e^{- \frac{G}{2w} t}\right] \qquad (3.3.9)$$

To determine the maximum height of saltation, from equation (3.3.9)

$$\frac{dy}{dt} = \frac{M - 1}{M} \frac{d}{\alpha} \left[-\left(- k \sin kt + \cos kt\right) e^{- \frac{G}{2w} t} + \right.$$

$$\left. \frac{G}{2w} e^{- \frac{G}{2w} t} \left(\cos kt + \frac{1}{k} \sin kt\right)\right]$$

For maximum y the velocity dy/dt must be equal to zero, and thus:

$$y_{max} = \frac{M - 1}{M} \frac{d}{\alpha} \tag{3.3.10}$$

Trying to model the movement as saltation, the maximum height reached for the particles must certainly be represented. From (3.3.10)

$$\alpha \left(\frac{y_{max}}{d} \right) = 1 - \frac{1}{M}$$

and recalling that $M = \frac{u_*^2}{u_{*c}^2}$ and $f\left(\frac{y}{d} \right) = 1 - \alpha\left(\frac{y}{d} \right)$,

$$f\left(\frac{y}{d} \right) = 1 - \alpha\left(\frac{y_{max}}{d} \right) = \frac{1}{M} = \frac{u_{*c}^2}{u_*^2} \tag{3.3.11}$$

is obtained. In order to keep the ratio between lift force and submerged weight constant, the function f(y/d) has to be equal in model and prototype:

$$\left(\frac{u_{*c}^2}{u_*^2} \right)_r = 1 \tag{3.3.12}$$

Considering water as the prototype fluid and air as the model fluid, equation (3.3.12) can be transformed to:

$$(\beta)_r = 8.75 \tag{3.3.13}$$

in accordance with the findings of the discussion on initiation of movement, equation (3.1.8).

To obtain the complete set of parameters governing the sediment

motion in the y direction, let us scale equation (3.3.7), using a vertical scale L_v, a time scale T_v and a particle settling velocity scale W. The following relations are obtained:

$$\frac{L_v}{T_v^2}\frac{1}{g}\left(\frac{\rho_s + k_2\,\rho_f}{\rho_s - \rho_f}\right) \quad , \quad \frac{u_*^2}{u_{*c}^2} \quad , \quad \alpha\,\frac{L_v}{d}\frac{u_*^2}{u_{*c}^2} \quad , \quad \frac{L_v}{T_v W}$$

Since α is a coefficient that gives the form of variation of the lift force with height, it can be considered equal in model and prototype; with the same scale for the sediment size and vertical dimensions, and observing that the last relation is a kinematic parameter, the relations are reduced to the two parameters:

$$\left[\frac{L_v}{T_v^2 g}\left(\frac{\rho_s + k_2\,\rho_f}{\rho_s - \rho_f}\right)\right]_r = 1$$

$$\left[\frac{u_*^2}{u_{*c}^2}\right]_r = 1 \qquad (3.3.14)$$

where the second parameter in the case of water as fluid in prototype and air as the model fluid can be written as $\beta_r = 8.75$, giving a modelling of the maximum height of saltation.

2. Sediment motion in the x direction

The equation of sediment motion in the x direction can be written as:

$$m\frac{d^2x}{dt^2} - D(s)\frac{\left(u - \frac{dx}{dt}\right)}{\frac{ds}{dt}} = 0 \qquad (3.3.15)$$

which can be transformed into

$$m \frac{d^2x}{dt^2} - \frac{W\ (u - \frac{dx}{dt}\ )}{w} = 0$$

dividing by W and using equations (3.3.4) and (3.3.5), we obtain

$$\frac{1}{g}\ (\ \frac{\rho_s + k_2\ \rho_f}{\rho_s - \rho_f}\ )\ \frac{d^2x}{dt^2} + \frac{1}{w}\frac{dx}{dt} - \frac{u}{w} = 0 \qquad (3.3.16)$$

Scaling this equation, using a horizontal scale L_h, a time scale T_h, a mean flow velocity scale U, and a mean particle settling velocity scale W, the following two parameters are obtained,

$$[\ \frac{L_h}{T_h{}^2 g}\ (\ \frac{\rho_s + k_2\ \rho_f}{\rho_s - \rho_f}\ )\ ]_r = 1 \qquad (3.3.17)$$

$$(\ \frac{U}{w}\ )_r = 1$$

Nordin and Beverage (50) discussed the validity of a ballistic trajectory approach for sediments moving as bed load in water, as used by Yalin (20) and followed in this study. They pointed out that apparently Yalin's bed load formula proportions the total load for low shear stresses or lower unit discharges. This finding can be explained since at these discharges the sediment in suspension does not account for much of the total load.

3.3.2. Summary of the similitude parameters

Time scales:

$$T_{h_r} = \left[\frac{L_h}{g} \left(\frac{\rho_s + k_2 \rho_f}{\rho_s - \rho_f} \right) \right]_r^{1/2}$$

$$T_{v_r} = \left[\frac{L_v}{g} \left(\frac{\rho_s + k_2 \rho_f}{\rho_s - \rho_f} \right) \right]_r^{1/2}$$

Velocity scales:

$$U_r = U_{*r} = \left(\frac{L_h}{T_h} \right)_r = \left[g L_h \left(\frac{\rho_s - \rho_f}{\rho_s + k_2 \rho_f} \right) \right]_r^{1/2}$$

Fluid discharge per unit width:

$$q_r = (U L_v)_r = \left[\left(g L_h \frac{\rho_s - \rho_f}{\rho_s + k_2 \rho_f} \right)^{1/2} L_v \right]_r$$

Total fluid discharge:

$$Q_r = (U L_v L_h)_r = \left[\left(g \frac{\rho_s - \rho_f}{\rho_s + k_2 \rho_f} \right)^{1/2} L_h^{3/2} L_v \right]_r$$

Defining a two-dimensional concentration, C_2, equal to the total fluid transverse area divided by the sediment are:

$$C_{2_r} = \left(\frac{L_h \, L_v}{d^2} \right)_r$$

With a three-dimensional definition of the concentration, C_3, equal to a fluid volume divided by the sediment volume:

$$C_{3_r} = \left(\frac{L_h^{\,2} \, L_v}{d^3} \right)_r$$

The mass of sediment ratio

$$(m_{s_2})_r = (\rho_s \, C_2 \, d^3)_r = [\rho_s \, L_h \, L_v \, d]_r$$

$$(m_{s_3})_r = (\rho_s \, C_3 \, d^3)_r = [\rho_s \, L_h^{\,2} L_v]_r$$

The sediment discharge per unit width

$$(q_{s_2})_r = \left(\frac{m_{s_2}}{\rho_s \, t_h \, L_h} \right)_r = \left[L_v d \left(\frac{g}{L_h} \cdot \frac{\rho_s - \rho_f}{\rho_s + k_2 \, \rho_f} \right)^{1/2} \right]_r$$

and the total sediment discharge

$$(Q_s)_r = \left(\frac{m_{s_3}}{\rho_s \, t_h} \right)_r = \left[L_v \, L_h^{\,3/2} \left(g \cdot \frac{\rho_s - \rho_f}{\rho_s + k_2 \, \rho_f} \right)^{1/2} \right]_r$$

The initiation of movement parameter β, when using the same fluid in model and prototype, is $\beta_r = 1$, and, when using air to model the movement of sediment by water, $\beta_r = 8.75$. The velocity ratio $\left(\frac{U}{w} \right)_r = 1$.

3.4. Suspension and wash load movement

3.4.1. Primary requirement

1. Basic equations

The mass conservation equation for sediments with a concentration $c(x,y,z,t)$ can be written in a Cartesian coordinate system:

$$\frac{\partial c}{\partial t} + u\frac{\partial c}{\partial x} + v\frac{\partial c}{\partial y} + w\frac{\partial c}{\partial z} = \frac{\partial}{\partial x}\left(E_x\frac{\partial c}{\partial x}\right) + \frac{\partial}{\partial x}\left(E_y\frac{\partial c}{\partial y}\right) + \frac{\partial}{\partial z}\left(E_z\frac{\partial c}{\partial z}\right) + w_s\frac{\partial c}{\partial y} \qquad (3.4.1)$$

where: u,v,w are time averaged components of instantaneous velocity in the x, y and z directions respectively; E_x, E_y and E_z are the turbulent diffusion coefficients; $u\frac{\partial c}{\partial x}$, $v\frac{\partial c}{\partial y}$, $w\frac{\partial c}{\partial z}$ are changes of concentration by convection; $\frac{\partial}{\partial x}\left(E_x\frac{\partial c}{\partial x}\right)$, $\frac{\partial}{\partial y}\left(\frac{\partial c}{\partial y}\right)$ and $\frac{\partial}{\partial z}\left(E_z\frac{\partial c}{\partial z}\right)$ are changes in the flux of the sediments by turbulent diffusion; $w_s\frac{\partial c}{\partial y}$ represents the settling of the sediments and w_s is the mean fall velocity of the sediments. From equation (3.4.2) on w_s will be referred to as w.

Taking the direction of flow as that of increasing x, the y axis directed upward from the bottom, and z a lateral direction.

Considering:

- a wide channel, the rate of change is smaller in the z direction, i.e.

$$\frac{\partial}{\partial y} > \frac{\partial}{\partial x} >> \frac{\partial}{\partial z}$$

- a slowly varying flow, with the diffusion of sediments in the longitudinal x direction smaller than in the vertical y direction, i.e.

$$\frac{\partial}{\partial x}\left(E_x \frac{\partial c}{\partial x}\right) << \frac{\partial}{\partial y}\left(E_y \frac{\partial c}{\partial y}\right)$$

- the vertical and lateral components of the mean flow velocity v and w are equal to zero.

The equation (3.4.1) reduces to:

$$\frac{\partial c}{\partial t} + u \frac{\partial c}{\partial x} = \frac{\partial}{\partial y}\left(E_y \frac{\partial c}{\partial y}\right) + w \frac{\partial c}{\partial y} \qquad (3.4.2)$$

For fully developed turbulent flow, the turbulent diffusion coefficient per momentum E_{my} can be written:

$$E_{my} = \frac{\tau/\rho}{du/dy} \qquad (3.4.3)$$

Considering a linear shear stress distribution which holds strictly only for a uniform and steady flow of uniform density

$$\tau = \tau_o \, (1 - y/y_o) \qquad (3.4.4)$$

the Karmán-Prandtl velocity distribution profile

$$\frac{du}{dy} = \frac{\sqrt{\tau_o/\rho}}{ky} \qquad (3.4.5)$$

and with $\sqrt{\tau_o/\rho}$ we obtain from (3.4.3) making use of equations (3.4.4) and (3.4.5):

$$E_{my} = k \, u_* \, y(1 - y/y_o) \qquad (3.4.6)$$

with $\eta_o = y/y_o$, equation (3.4.6) is written:

$$\frac{E_{my}}{u_* y_o} = k\,\eta_o(1 - \eta_o) \tag{3.4.7}$$

Many investigators have related the turbulent diffusion coefficients per mass and per momentum by a constant of proportionality λ in the form: $E_y = \lambda E_{my}$, where λ can vary from values less than unity to larger than unity. λ depends on many factors, such as size of material bed formations (52), relation between sediment and fluid densities (53) and some other factors like sediment concentration and fluid viscosity, but nevertheless it can always be written:

$$E_y = \lambda\, k\, u_*\, y_o\, \eta_o\, (1 - \eta_o) \tag{3.4.8}$$

Therefore the ratio between these turbulent mass transfer coefficients for the prototype and model can be reduced to:

$$(E_y)_r = \frac{[\lambda\, k\, u_*\, y_o\, \eta_o\, (1 - \eta_o)]_p}{[\lambda\, k\, u_*\, y_o\, \eta_o\, (1 - \eta_o)]_m} = (u_*\, L_v)_r \tag{3.4.9}$$

With this definition of the turbulent mass transfer coefficient, steady motion ($\partial/\partial t = 0$), and unsteady motion, considering very gradual variation with time, will be discussed.

a. Steady and uniform flow, in this case $\partial/\partial x = 0$ and the governing equation is:

$$\frac{\partial}{\partial y}\left(E_y \frac{\partial c}{\partial y}\right) + w \frac{\partial c}{\partial y} = 0$$

Assuming the particle mean fall velocity to be independent of the concentration, although McNown and Lin (54) and Coronado (55), among others, have demonstrated experimentally that w is a function of the concentration, the well-known O'Brien formula (56) is obtained,

$$wc + E_y \frac{\partial c}{\partial y} = 0 \qquad (3.4.10)$$

b. Steady and non-uniform flow, then the governing equation is:

$$u \frac{\partial c}{\partial x} - w \frac{\partial c}{\partial y} = \frac{\partial}{\partial y} \left(E_y \frac{\partial c}{\partial y} \right) \qquad (3.4.11)$$

c. Unsteady and non-uniform flow, governed by equation (3.4.2).

2. Similitude analysis

Considering C a reference concentration, U and w, characteristic velocities; L_v and L_h characteristic vertical and horizontal scales; T a reference time; $( )^o$ a dimensionless quantity, and $( )_r$ the ratio between prototype and model values, the governing equations can be scaled for the cases presented.

a. Steady and uniform flow, introducing the reference values in equation (2.4.10)

$$wC \ (w^\circ \ c^\circ) + \frac{CE_y}{L_v} \left(\frac{\partial c^\circ}{\partial y^\circ} \right) = 0$$

is obtained. After multiplying by L_v/CE_y, the dimensionless parameter

$$\frac{wL_v}{E_y}$$

is obtained. Determining the scale ratios for similarity and using the result (3.4.9), $(w/u_*)_r = 1$ results.

Using the velocity distribution $U = u_* f_1(u_* d/\nu)$, as written in section 2.1, the following parameter

$$\left(\frac{w}{U}\right)_r = 1 \qquad (3.4.12)$$

is obtained.

b. Steady and non-uniform flow, introducing the reference values in the corresponding governing equation

$$\frac{UC}{L_h}\left(u^\circ \frac{\partial c^\circ}{\partial x^\circ}\right) - \frac{wC}{L_v}\left(w_s{}^\circ \frac{\partial c^\circ}{\partial y^\circ}\right) = \frac{1}{L_v}\frac{\partial}{\partial y^\circ}\left[E_y \frac{C}{L_v}\left(\frac{\partial c^\circ}{\partial y^\circ}\right)\right]$$

after multiplying by L_h/UC, we obtain the dimensionless parameters:

$$\frac{wL_h}{UL_v} \qquad \text{and} \qquad \frac{E_y L_h}{U L_v{}^2}$$

Determining the scale ratios for similarity, and assuming similarity of velocity distributions for non-uniform flow to exist and thus introducing equation (3.4.9) in the second parameter, we can conclude that we must have the horizontal scale equal to the vertical scale, that is, vertical distortion is not possible. The dimensionless parameters reduce to

$$\left(\frac{w}{U}\right)_r = 1 \qquad (3.4.13)$$

c. Unsteady, non-uniform flow can only be analyzed if the variation

with time is very gradual, as in the case of tidal motions, so that the shear stress and velocity distributions of uniform flow are approximately valid. Scaling equation (3.4.2)

$$\frac{C}{T}\left(\frac{\partial c^\circ}{\partial t^\circ}\right) + \frac{UC}{L_h}\left(u^\circ \frac{\partial c^\circ}{\partial x^\circ}\right) - \frac{wC}{L_v}\left(w^\circ \frac{\partial c^\circ}{\partial y^\circ}\right) = \frac{1}{L_v}\frac{\partial}{\partial y^2}\left[E_y \frac{C}{L_v}\left(\frac{\partial c^\circ}{\partial y^\circ}\right)\right]$$

and after multiplying by T/C the following dimensionless parameters are obtained:

$$\frac{UT}{L_h} \quad , \quad \frac{wT}{L_v} \quad , \quad \frac{E_y T}{L_v^2}$$

The first of these is a kinematic parameter. Multiplying by L_h/UT, the three parameters result in the form:

$$\frac{L_h}{U_T} \quad , \quad \frac{w}{U}\frac{L_h}{L_v} \quad , \quad \frac{E_y T}{L_v^2}$$

the first parameter is again kinematic, the other two can be reduced to:

$$\left(\frac{w}{U}\right)_r = 1$$

The mean fall velocity can be obtained from Figs. 7 and 8, taken from reference (40).

3.4.2. Secondary requirement

In the case of steady uniform flow, the mean fluid velocity, which is one of the main independent variables affecting the sediment movement, can be obtained from the Darcy-Weisbach equation with D = 4R:

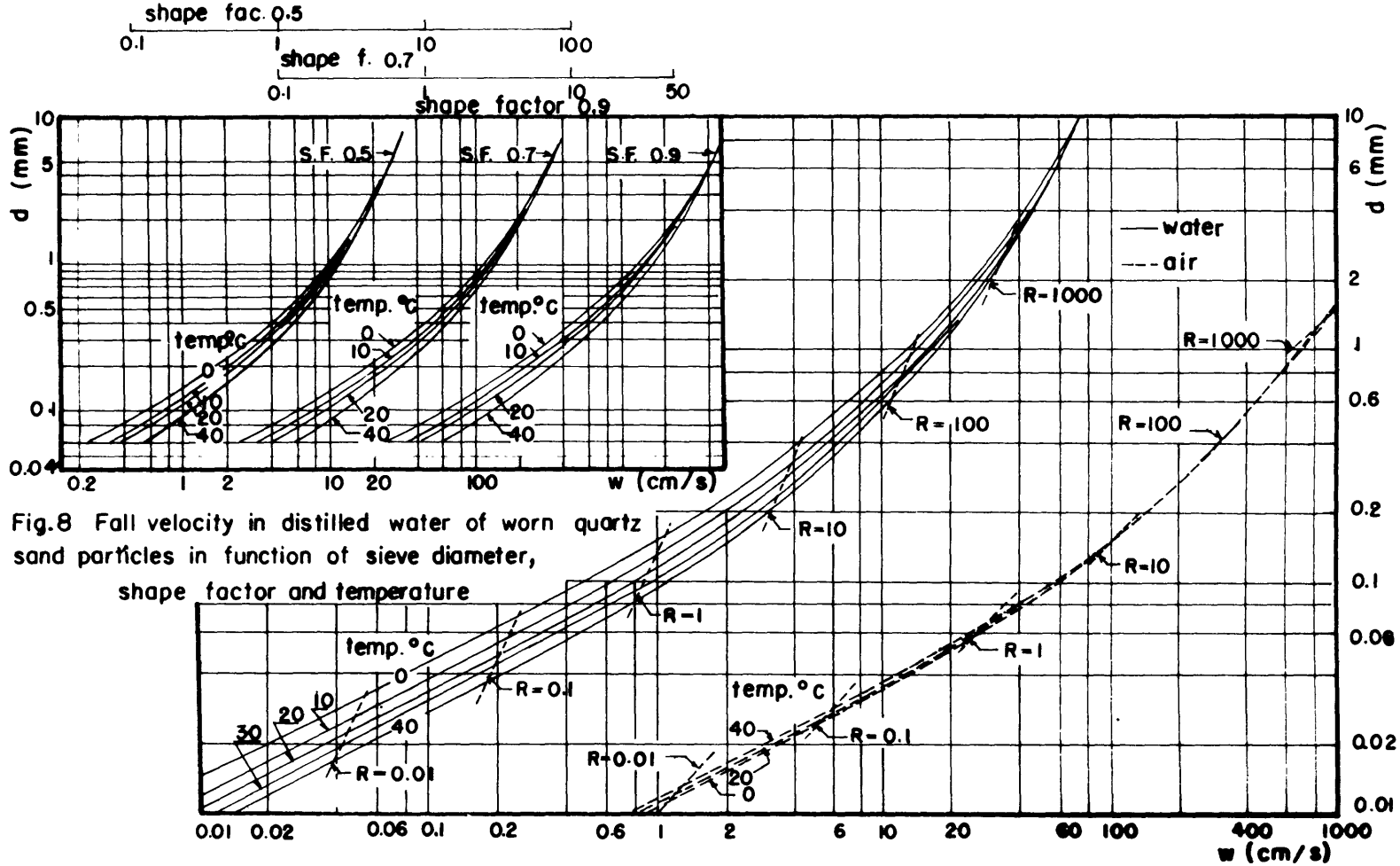

Fig.8 Fall velocity in distilled water of worn quartz sand particles in function of sieve diameter, shape factor and temperature

Fig.7 Fall velocity of quartz spheres in air and water. Rouse (40)

$U = \sqrt{8g/f}\ \sqrt{RS}$. This equation of the mean velocity gives for similarity:

$$U_r = \left[\frac{RL_v}{fL_h} \right]_r^{1/2} \qquad (3.4.14)$$

where f_r is the ratio between the friction factors in model and prototype.

Following Meyer-Peter and Müller (17) in dividing the friction factor into a grain friction f' and a bed form friction f", we can write:

$$f_r = \frac{f'_m + f''_m}{f'_p + f''_p} \qquad (3.4.15)$$

Until recently, the Moody diagram was accepted for the calculations of f' (57) although this diagram was plotted from experiments over fixed walls. Alam, Cheyer, and Kennedy (58) noted that even when the friction factor calculated with a Moody diagram has values higher than for bed with sediment in movement, these differences are small and not known. The representative k_e may be replaced by d_{50}, the particle diameter with 50% of finer elements.

Earlier, Ippen and Verma (45), for flow over a rough bed with moving particles calculated values for f' confirming the Moody diagram trend for Reynolds numbers less than 10^5, but, from their correlation between the Manning coefficient n, Reynolds number and the relative roughness R/k_e, it is possible to observe an increase in the values of n for Reynolds numbers larger than 2.5×10^4. Knowing that the friction factor f can be written as proportional to the square of the Manning coefficient, it is possible to expect an increasing trend for values of the friction factor

f' for higher Reynolds numbers.

Recently, Lovera and Kennedy (59) presented the friction factor f' in the form

$$f' = f\left(\frac{uR}{\nu}, \frac{R}{d_{50}}\right)$$

Plotting experimental flow and natural river data, they show that for Reynolds numbers larger than 2.5×10^4, f' increases with the Reynolds number as can be seen in Figs. 9 and 10. For lower Reynolds numbers the Moody diagram may be used (Fig. 11).

The bed form friction factor f" can be obtained from Fig. 12 taken from reference (58). The approach used in the last mentioned reference is reinforced by J. Herbertson (60) who performed an analysis very similar to Alam, Cheyer and Kennedy (58).

The procedure to obtain the velocity ratio from formula (3.4.14) can be one of trial and error. Assuming a model fluid flow velocity, the friction factors f'_m and f''_m are calculated, then the friction factors ratio f_r can be determined. The velocity ratio U_r using the Darcy equation is recomputed and checked with the first assumption.

In the case of wide channels, equation (3.4.14) reduces to

$$U_r = \left(\frac{L_v^2}{fL_h}\right)_r^{1/2} \qquad (3.4.15)$$

For the cases of unsteady and steady non-uniform flow, the dynamic equation of motion for an open channel is:

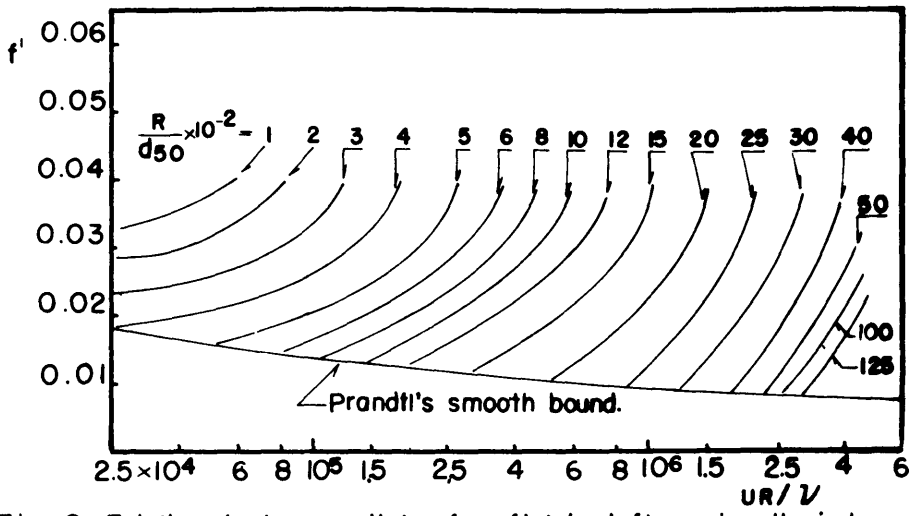

Fig. 9 Friction factor predictor for flat bed flows in alluvial channels. Lovera, Kennedy (59)

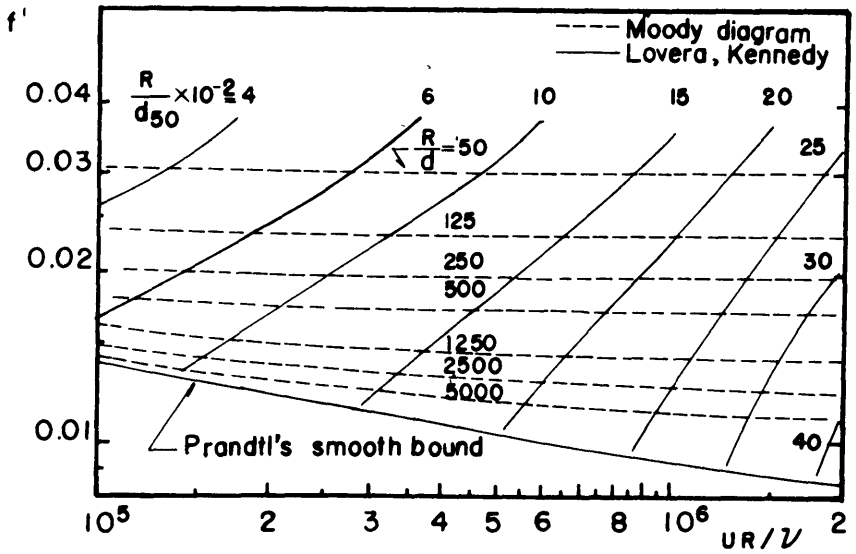

Fig. 10 Comparison of friction factors for flows in uniform rigid boundary conduits and flat bed alluvial channels (59)

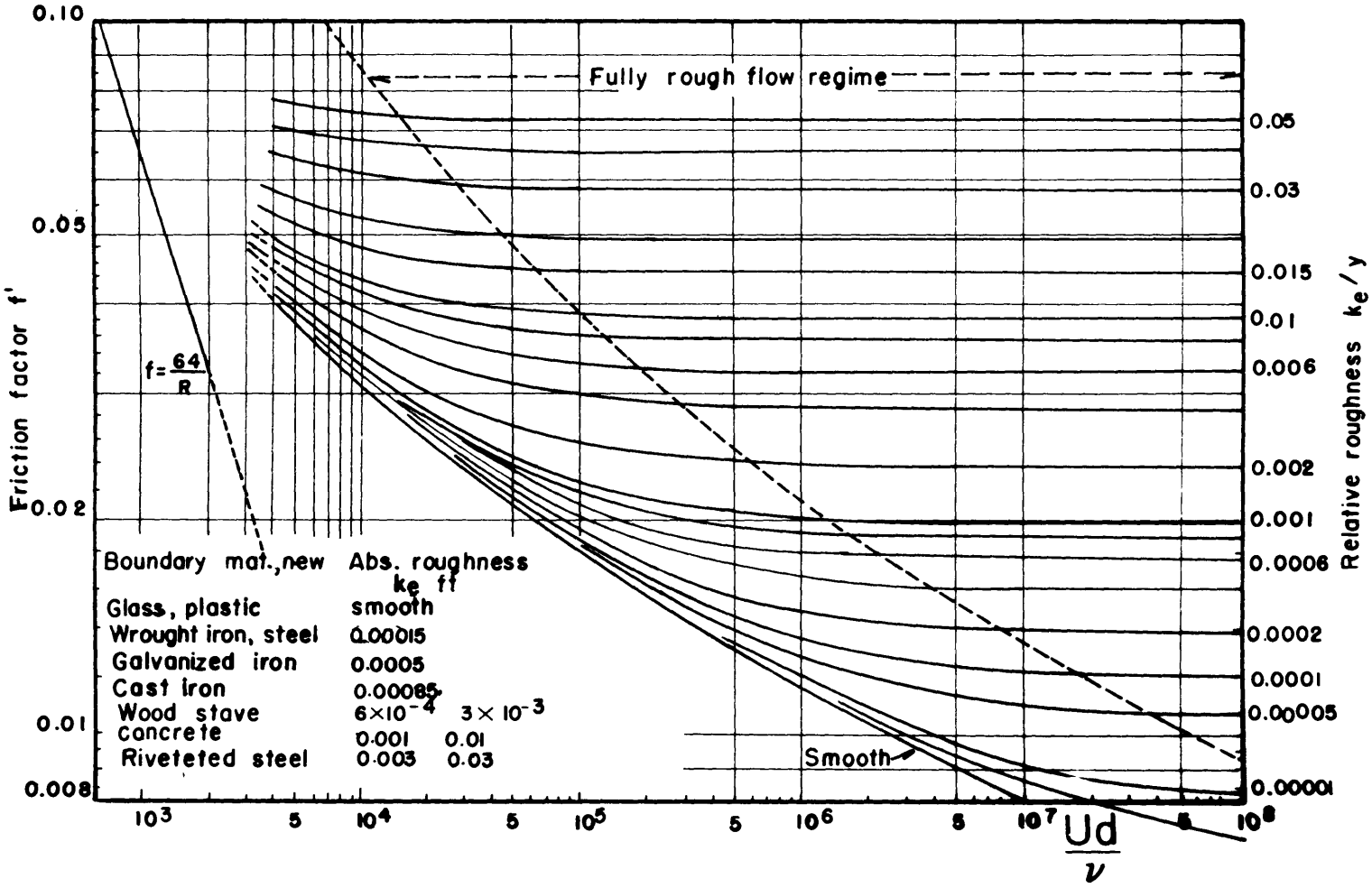

Fig. II Moody diagram

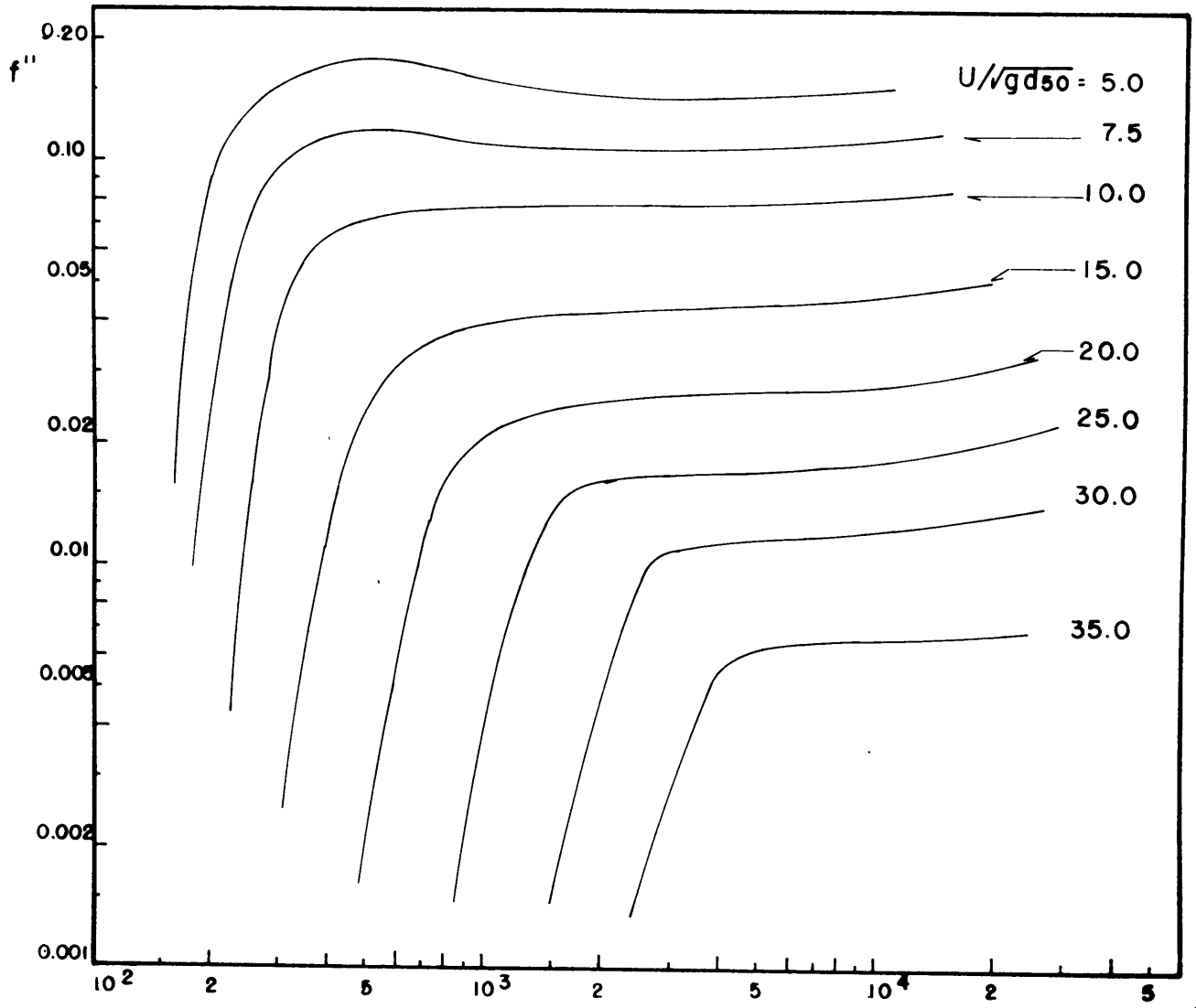

Fig 12 Form drag friction factor in sand bed channels, f''. Alam, Cheyer, Kennedy (58)

$$\frac{\partial u}{\partial t} + \alpha\, v\, \frac{\partial u}{\partial x} = -g\left[\frac{\partial y_o}{\partial x} - S_o\right] - g\, S_f \qquad (3.4.16)$$

After scaling, this equation transforms to:

$$\frac{U}{T}\left(\frac{\partial u^\circ}{\partial t^\circ}\right) + \left(\alpha\, \frac{U^2}{L_h}\right)\left(u^\circ\, \frac{\partial u^\circ}{\partial x^\circ}\right) = -\, g\left[\frac{L_v}{L_h}\frac{\partial y^\circ}{\partial x^\circ} - \frac{L_v}{L_h}\, S_o{}^\circ\right] - g\, S_f$$

which gives the following dimensionless parameters after multiplying by L_h/U^2

$$\frac{L_h}{U_T}\ ,\ \alpha\ ,\ \frac{gL_v}{U^2}\ ,\ \frac{gL_h}{U^2}$$

The α_r can be equated to 1 since their values are very close to 1. Under undistorted conditions the Froude Law velocity ratio results:

$$U_r = L_r{}^{1/2} \qquad (3.4.17)$$

3.4.3. Summary of the similitude parameters

Time scale. Steady uniform flow

$$T_r = \left(\frac{f\, L_h{}^3}{R\, L_v}\right)_r^{1/2}$$

Gradually varied flow and unsteady flow

$$T_r = L_r{}^{1/2}$$

Fluid discharge. Steady uniform flow

per unit width

$$q_r = (U\ L_v)_r = \left(\frac{L_v^4}{fL_h}\right)_r^{1/2}$$

total discharge

$$Q_r = (U\ L_v\ L_h)_r = \left(\frac{R\ L_v^3\ L_h}{f}\right)_r^{1/2}$$

Gradually varied and unsteady flows

per unit width

$$q_r = L_r^{3/2}$$

total discharge

$$Q_r = L_r^{5/2}$$

Sediment discharge. Using the definition of concentrations, masses and sediment discharge as defined for the case of bed load and saltation.

For steady uniform flow

per unit width

$$q_{s_r} = \left(\frac{m_{s_2}}{\rho_s\ t\ L_h}\right)_r = \left(\frac{d^2 L_v^4}{f\ L_h^3}\right)_r^{1/2}$$

total discharge

$$Q_{s_r} = \left(\frac{m_{s_3}}{\rho_s\ t}\right)_r = \left(\frac{R\ L_v^3 L_h}{f}\right)_r^{1/2}$$

For gradually varied and unsteady flows

per unit width

$$q_{s_r} = (dL^{1/2})_r$$

total discharge

$$Q_{s_r} = L_r^{5/2}$$

The velocity ratios; for all cases

$$\left(\frac{w}{U}\right)_r = 1$$

The velocity scales

Steady uniform flow

$$U_r = \left(\frac{R\, L_v}{f\, L_h}\right)_r^{1/2}$$

Gradually varied and unsteady flows

$$U_r = L_r^{1/2}$$

3.5. Local scour

The understanding of the mechanism of the sediment transport in uniform steady flow is difficult in itself. The process of localized scour presents additional complications due to the change of flow characteristics with time, or some particular fluid pattern due to the effect of the

geometry of some obstacle. In this situation, a general solution or an equation that could describe the process is practically impossible.

Rouse (31) and Laursen (61) presented the parameters wt/ℓ and U/w as the characteristics for the development of local scour produced by horizontal and vertical jets. Laursen (62), (63) proposed some expressions for different cases of localized scour, but there is, as yet, no consistent generalization for a model study. Carstens (64), analyzing the equilibrium of a single particle, obtained a parameter $u/\sqrt{(\rho_s/\rho_f-1)gd}$ that can be transformed to the Shields parameter following the previous consideration for initiation of motion of sediments. Field (33), with dimensional analysis, found, among many other dimensionless numbers, a parameter similar to that obtained by Carstens.

In the present study the local scour patterns developed were initially assumed to depend on the following characteristics:

The parameter (U/w) is assumed as significant here as it was obtained from studying the movement of sediment as bed load and in suspension.

It can also be concluded that the initial shear stress τ_o responsible for the development of a scour pattern must be significant relative to the critical shear stress τ_c as defined by Shields. Therefore, the scour dimensions should be dependent on τ_c/τ_o or β_c/β according with equation (3.1.8).

Finally, the time passed until a stable scour pattern is obtained may be related to the time ratio developed for the saltation model (see section 3.3.1).

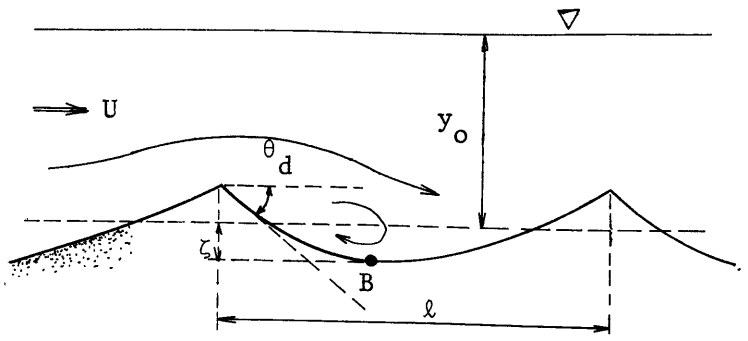

Fig. 13. Characteristic scour geometry

Following the notations defined in Fig. 13 a general relation for the relative scour depth ξ/ℓ may thus be written as:

$$\xi/\ell = f\left(\frac{u}{w} , \frac{\beta}{\beta_c} , \frac{1}{t} \left(\frac{L}{g} \frac{\rho_s + k_2 \rho_f}{\rho_s - \rho_f} \right)^{1/2} \right) \qquad (3.5.1)$$

It may be noted here that dunes and ripples in streamflow may be considered as a series of local scour patterns. For dunes and ripples Yalin (65) has found the length to depth ratio $\ell/y_o \approx 5$ while Nordin (66) obtained for the same ratio a constant of 4.2. This would point to scour being independent of the first two parameters of the function (3.5.1).

3.6. General modelling scheme

3.6.1. Procedure

Fig. 14 shows the steps to follow in order to choose the representative parameters for a model study of sediment movement.

The first step will be to check if the sediment will move. From comparison of the prototype Shields function β_p and the critical prototype value of the Shields function β_{pc}, there will be no sediment movement if

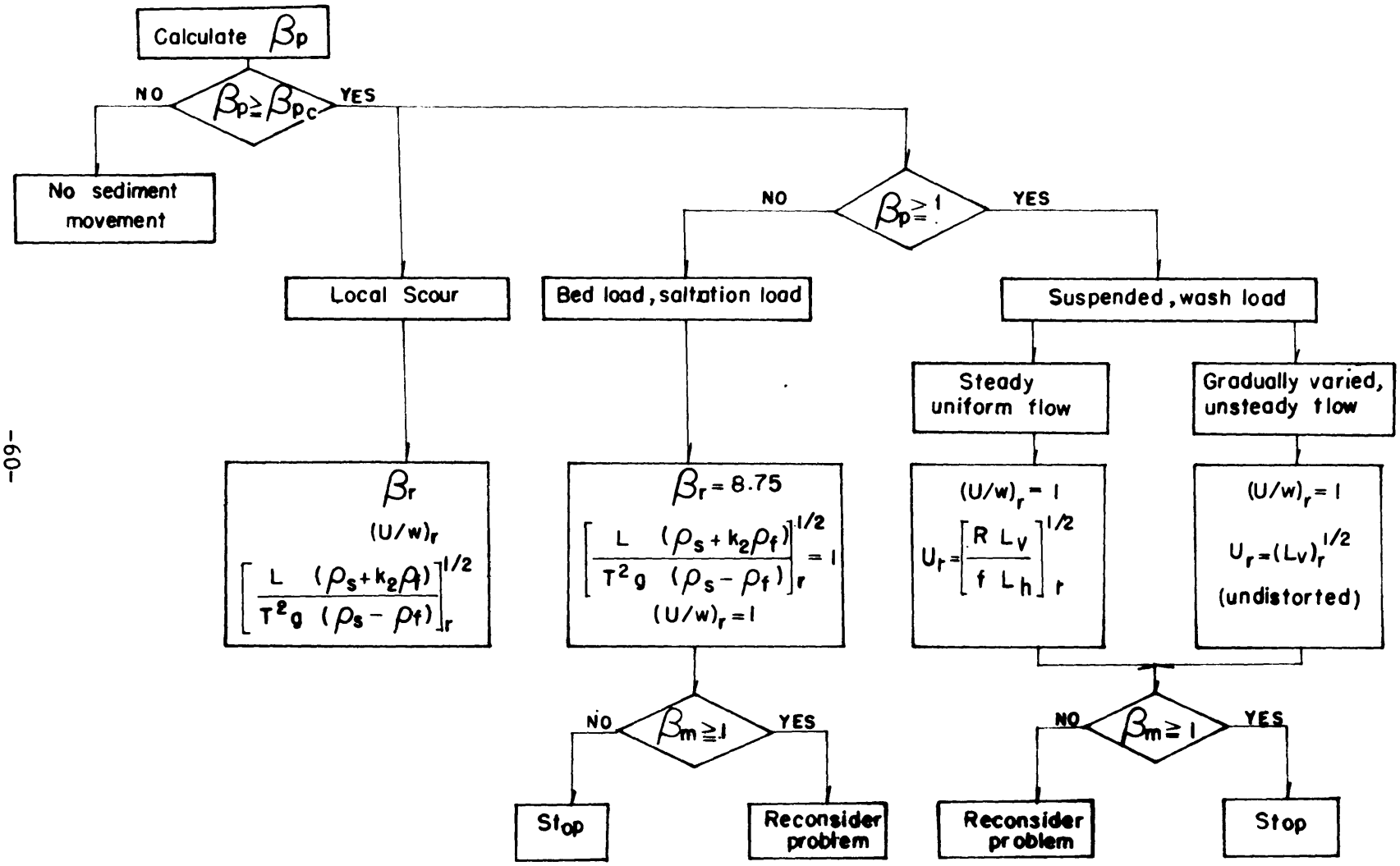

Fig. 14. General modelling scheme.

$\beta_p < \beta_{pc}$.

Since it is impossible to describe analytically in a unique form the total movement of sediment, the division of the modes of sediment motion primarily as bed load and saltation or as suspension and wash load can be made by comparing β_p with unity. If $\beta_p < 1$ the sediment will move as bed load and saltation, and if $\beta_p \geq 1$ the sediment will move primarily as suspension and wash load.

In the case of sediment movement as suspension and wash load the velocity scale can be chosen according to the kind of flow. For steady uniform and uniform varied flow $U_r = (RL_v/fL_h)_r^{1/2}$. For unsteady flow $U_r = Lv_r^{1/2}$.

The sediment discharge per unit of width is for bed load:

$$q_{sr} = Lv_r\, d_r \left[\frac{g}{L_h} \cdot \frac{\rho_s - \rho_f}{\rho_s + k_2 \rho_f} \right]_r^{1/2}$$

and for steady uniform flow with sediment in suspension.

$$q_{sr} = \left(\frac{d^2 L_v^4}{fL_h^3} \right)_r^{1/2}$$

and for non-uniform and gradually varied flows with sediment in suspension:

$$q_{sr} = (dL_v^{1/2})_r$$

The process of local scour can be studied in the case of long stretches of streams of movable bed by using the parameters for bed load or for suspension. In special cases, like scour at bridge piers: $\beta_r = 1$,

$(U/w)_r = 1$ and $t_r = [(L_h/g)^{1/2}(\rho_s + k_2\,\rho_f)^{1/2}/(\rho_s - \rho_f)^{1/2}]_r$ can be used.

3.6.2. Relation between the parameters characterizing the different modes of sediment movement

In the case of bed load and saltation the first relation to satisfy using the same fluid in model and prototype is $\beta_r = 1$, and using air as the fluid in the model $\beta_r = 8.75$.

If the Stokes formula for the fall velocity of the sediments applies:

$$w = \frac{1}{18}\frac{g}{\mu}(\rho_s - \rho_f)d^2$$

the Shields parameter can be written as:

$$\beta = \left(\frac{u_*}{w}\right)\frac{u_* d}{18\nu}$$

Since in the case of suspension and wash load the similarity ratio $(w/u)_r$ has to be equal to one, the parameters for modelling bed load and suspension are related by the Reynolds number ratio $\left(\frac{u_* d}{\nu}\right)_r$.

If the fall velocity follows the turbulent resistance relation at higher Reynolds numbers, it can be written as:

$$w = k\sqrt{(\rho_s - \rho_f)d}$$

where k is a coefficient of the particle shape depending on many factors. In this case the Shields parameter is expressed as:

$$\beta = \left(\frac{u_*}{w}\right)^2\left(\frac{k^2\rho_f}{g}\right)$$

Only in the case of using the same fluid and particles in model and prototype can sediment movement be represented in the laboratory using either bed load or suspended load parameters.

IV. EXPERIMENTAL VERIFICATION

4.1. Scope of the experimental study

The purpose of the experimental tests is to verify the applicability of the similitude parameters derived in the study. However, the magnitude of the work that a verification of all these parameters would require limits the scope of the present study to the testing of one set of parameters. The particular case chosen for this purpose is a problem of local scour.

In this study, the action of a horizontal, two-dimensional jet of water, submerged in water, over an originally horizontal bed of sediments is considered and is compared with the action of a horizontal, two-dimensional jet of air, submerged in air.

This case already is quite complicated since the sediment moves as bed load as well as in suspension. Consequently, an experimental verification of the local scour parameters can be considered to be valid quite generally and may be expected to apply to different scour problems with different flow patterns.

Specifically, the experiments were designed to explore the action of a jet of water and of air issuing through a nozzle, .25 inches in height and 6 inches in width over an initially flat bed of uniform, granular sand. Three diameters of sand particles .71, .59 and .42 mm nominally were employed. Velocities could be varied from 40 to 78 cm/sec in water and from 9 to 27 m/sec in air. Scour patterns were observed for 16 tests with different values of velocities and grain diameters under

transient conditions up to the ultimate stable scour pattern.

4.2. Experimental setup

The equipment, designed and built for the present tests, consists of a main tank, water and air supply systems, auxiliary devices for flow measurement and control. Fig. 15 and Photographs 1 and 2 show this apparatus.

4.2.1. The experimental flume

The main tank, built in plexiglass 3/8 in. thick, is 6 in. wide and 78 in. long, and is divided into 3 chambers. The first one, a stilling chamber, is 14 in. long and 40 in. high. The fluid enters through a circular opening 3 in. in diameter in the bottom of this chamber. It serves as a constant head tank for the flow discharging to the second chamber through a horizontal slot 1/4 in. high and 6 in. wide, with its lower edge 10 in. high over the bottom of the tank.

The second chamber is 60 in. long and 28 in. high and is the main test chamber containing the sediment bed. A grid formed of one inch squares is inscribed on one of the lateral walls for observation of the scour patterns. This test chamber is connected to the third chamber over a suppressed weir 25 in. high that serves to keep the water jet under constant submergence. It also prevents the transport of sand into the pump sump. The third chamber is only 4 in. long and 28 in. high and essentially serves only as a return to the sump through a 2 in. diameter pipe.

The recirculating water system consists of a 15 gallon sump connected by a 1 in. pipe (PVC sch 40) to a constant discharge centrifugal pump

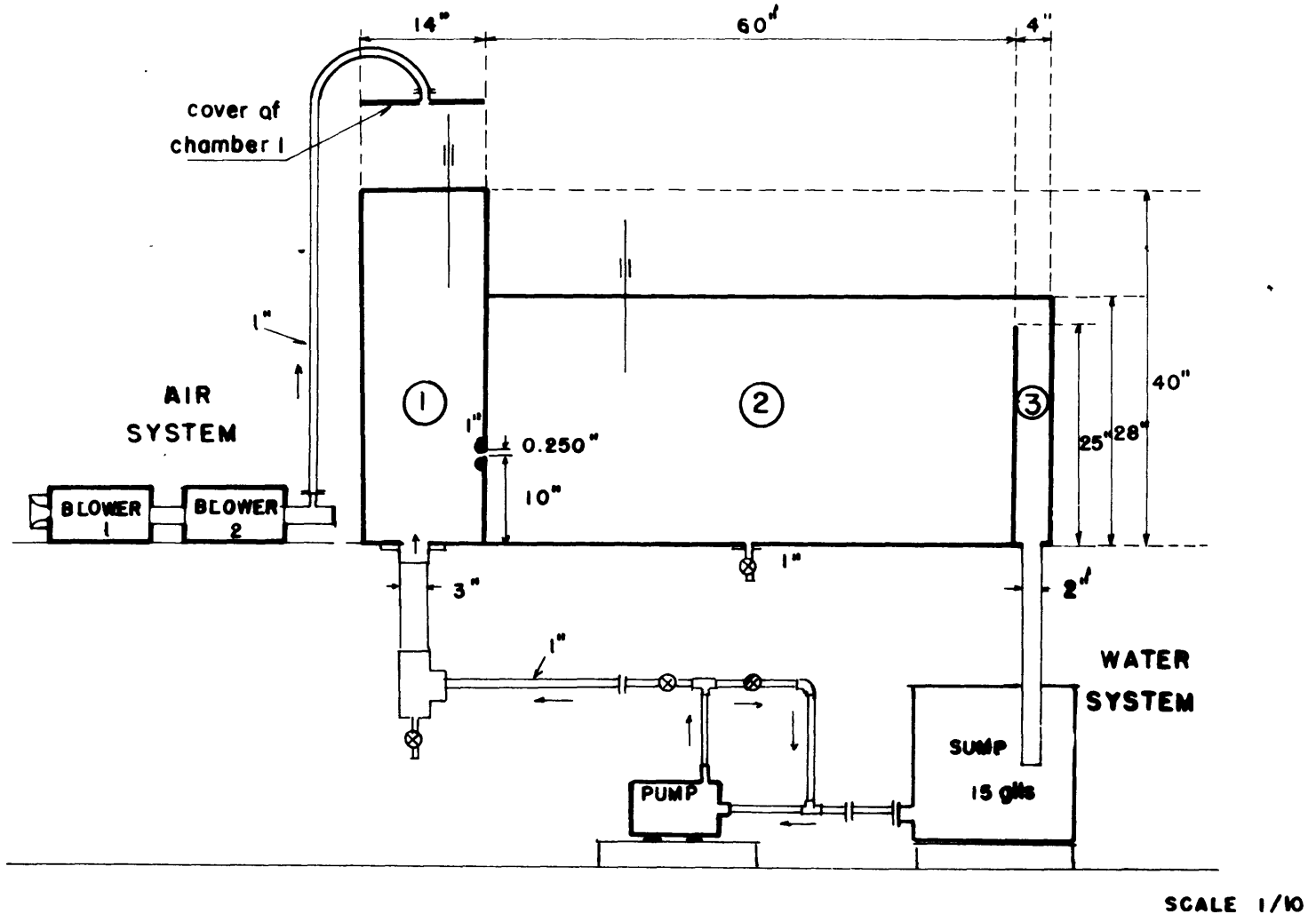

Fig. 15 Main tank and air and water supply systems

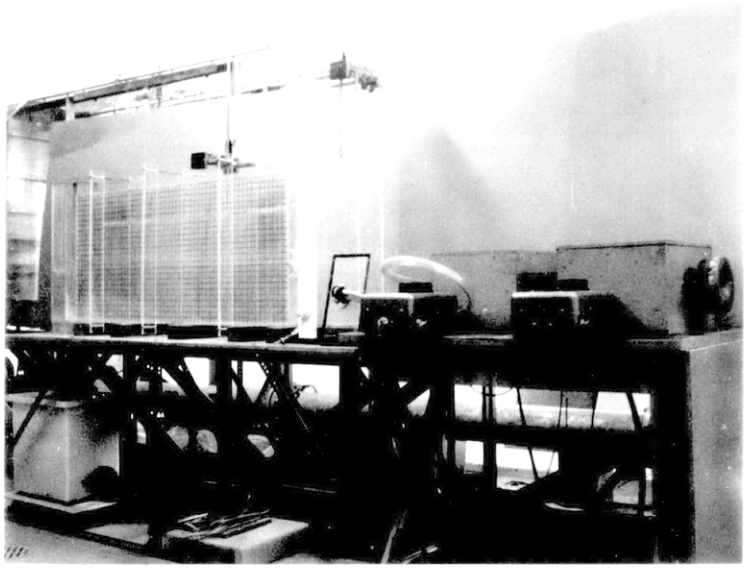

Photo 1. Main tank and air water system

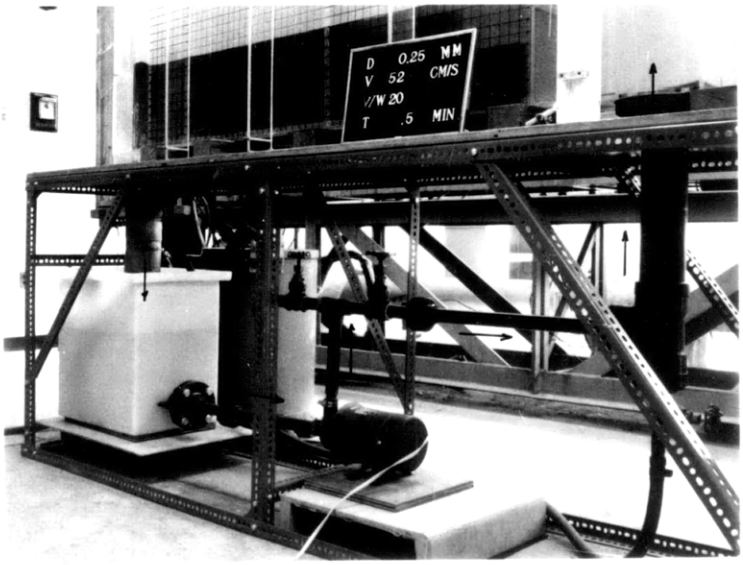

Photo 2. Water supply system

(Cole Palmer model 7006-1). This is powered by a 1/3 HP motor with 3450 RPM. A 1 in. pipe by-pass serves to regulate the water discharge toward the entrance tank.

The air supply system consists of 2 blowers installed in series. Each one consists of two self-cooling vacuum cleaner motor-fans enclosed in a 1/2 in. plywood wall, and rated at 1/3 to 1/2 HP at high speed operation. These motors have a variable voltage supply in the range 30 to 120 volts through a General Radio Corp. model W-20-M Variac transformer. The discharge control is complemented with a Butterfly valve installed at the end of a short 2 in. pipe, ahead of the air supply line.

4.2.2. Testing equipment

The flow measurement, in the case of the water jet, was obtained by measuring the water jet velocity passing through the horizontal slot, as a function of the differential water head. The zero level was considered at the top of the weir between the second and third chambers. This differential water head was measured with a point gage of 0.001 ft. divisions. Fig. 16 shows the calibration curve, which, for convenience, gives the jet velocity in terms of water surface elevation h above the weir crest.

For the air jet the different variac settings regulated the fluid discharge. A water manometer with readings of 1 mm, and connected to the first chamber, was used to measure the pressure inside that chamber, and after a transformation to an equivalent column of air, the air jet velocity is obtained using the relation $U = \sqrt{2gh}$ assuming no losses at the entrance to the second chamber where the scour was produced. Table 1

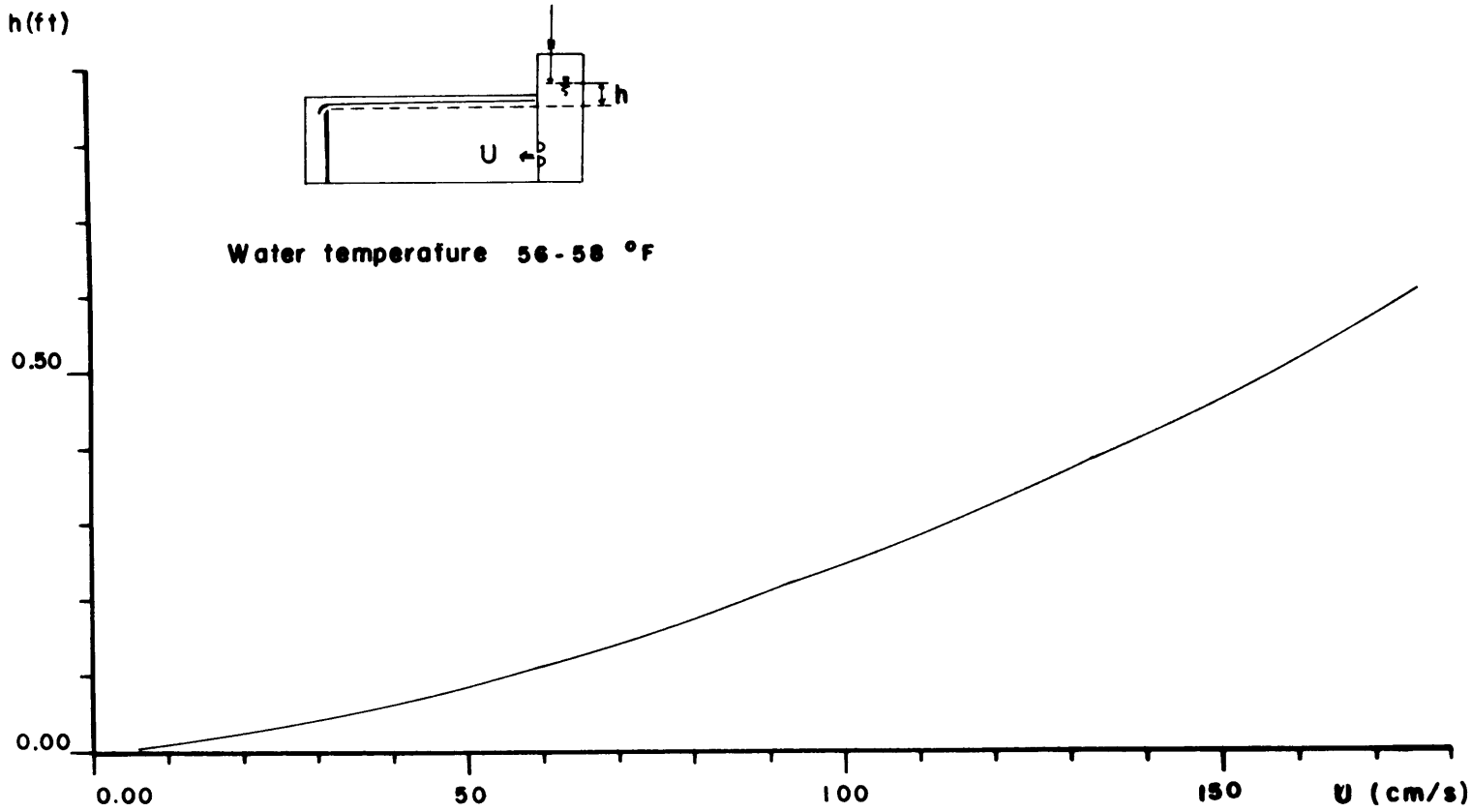

Fig. 16 Water jet velocity. Calibration curve

presents the values of chamber pressures in cm of water column against variac settings and jet velocities.

Table 1

Blower calibration. Water pressure vs. variac settings.

Δh(cm)	Variac Settings No. 1	No. 2	Velocity (m/s)
0.30	21.5	12.5	6.80
0.54	20	15	9.00
0.67	25	17.5	10.10
0.94	30	25	11.90
1.91	51	43	17.00
2.15	52.5	45	18.00
2.71	65	54	20.20
4.4	90	78	25.50
4.84	95	85	27.00
6.10	115	103	30.30
6.60	120	110	31.50

The scour measurements were obtained from photographs taken with a Polaroid Land 350 camera. The photographs showed the scour profile behind a grid with one inch squares. A point gage with 0.001 ft. accuracy was used directly on the scour profile to check the measurements on the photographs. Polaroid Land film, black and white, type 107, 3000 speed with 3-1/4 x 4-1/4 inch prints was used.

A thermometer, installed in the entrance chamber, measured the water temperature, and another, installed in the exit chamber, determined the room temperature for the air jet.

4.2.3. Sediment characteristics

Sand classified according to the U.S. Standard sieve series was used for the experiments. Sand passing the sieve no. 20, 0.84 mm opening, and retained on sieve no. 25, 0.71 mm opening, was labelled as 0.71 mm diameter, sand passing the sieve no. 25 and retained on sieve no. 30, 0.59 mm opening, as 0.59 mm diameter, and the sand passing the sieve no. 30 and retained on sieve no. 60, 0.25 mm opening, was labelled as 0.42 mm. The corresponding fall velocities were determined experimentally (listed in Table 2) and also from the ASCE publication (40).

Table 2 presents the specific gravity, fall velocity in still water, angle of repose and the grain shape for the different diameters of sand. The specific gravity was obtained by the picnometer method, the fall velocity with a settling vertical tube 5 ft. long and 2 in. inside diameter; the angle of repose was obtained by gentle pouring on a flat surface. The microscope observation indicated the quartz nature of the grains and their rounded shape. Photographs 3, 4, and 5 show these grains.

Table 2

Sand characteristics

d(mm)	Particle shape	Specific gravity	Fall velocity w(cm/s)				Angle of repose
			59°		63°		
			air	water	air	water	
.71	Rounded	2.73	505	10.45		11.40	29°22'
.59	Rounded	2.64	450	9.54		9.57	29°56'
.42	Rounded	2.67	315	6.72			30°43'

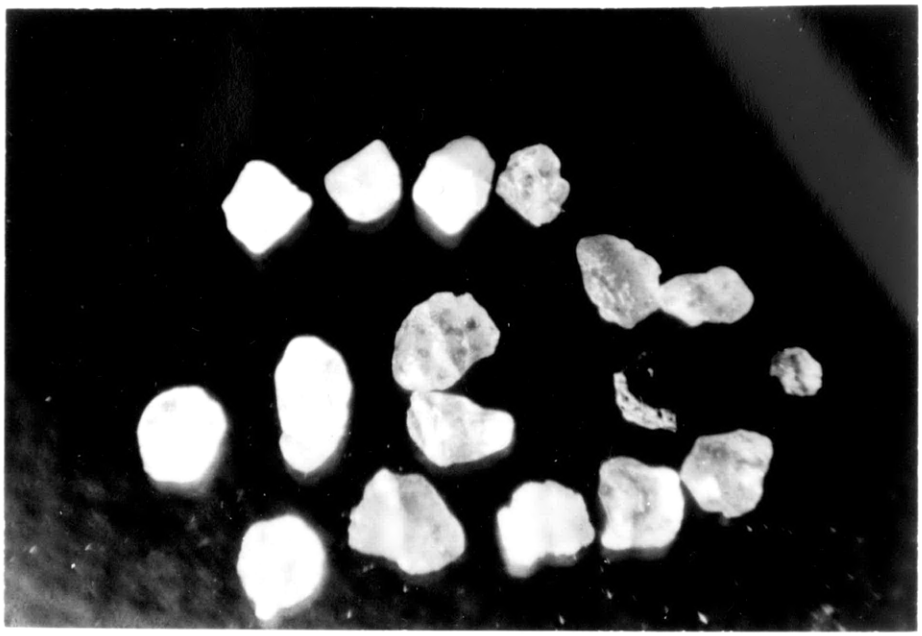

Photo 3. Sand varying between 0.84 mm and 0.71 mm and named as 0.71 mm

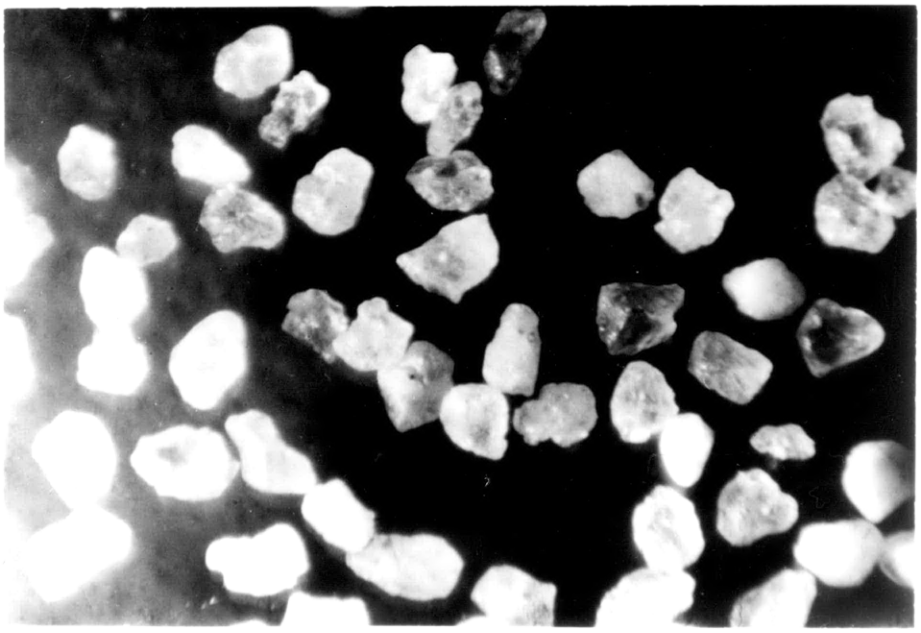

Photo 4. Sand varying between 0.71 mm and 0.59 mm and named as 0.59 mm

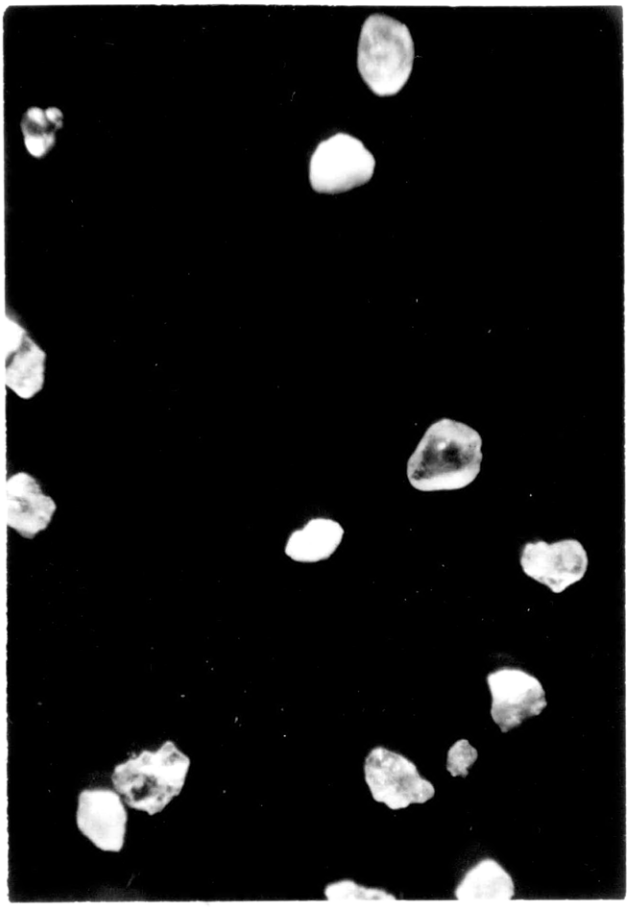

Photo 5. Sand varying between 0.59 mm and 0.25 mm and named as d=0.42 mm

4.3. Experimental procedure

The first step is to fill the second chamber until the level of the bottom of the horizontal slot located between the first and this second chamber is reached, in this case with a 10 inch high layer of one sediment size.

In the case of an air jet, after sealing the top of the first chamber, the next step is to supply air pressure, controlled by varying the variac settings. The water manometer gave the interior pressure and the air jet velocity using the calibration Table 1.

In the case of a water jet the second step is to fill the second chamber until the water level reaches the top of the wall located between the second and the third chamber. That will give a minimum of submergence of 15 inches. Water was then pumped into the first chamber with the nozzle initially closed to avoid passing of sand to the first chamber. The desired jet velocities are then obtained from reading the head of water over the top level of the weir between the second and the third chamber using the calibration curve previously shown.

These procedures, for the case of a jet of air as well as for a jet of water, were repeated with 3 different sand sizes. Three jet velocities were used on the 2 smaller sizes of particles 0.59 mm and 0.42 mm, and two jet velocities on the 0.71 mm particles.

To register the successive scour profiles, photographs were taken after 0.5, 1, 2, 5, 10, 15, 30, 60 minutes and every hour thereafter from the beginning of each run. Extra photographs were taken in some of the runs. From each photograph the vertical and horizontal coordinates of

the points of the scour profile were measured. The approximation on the reading was 1/20 inch. Fig. 17 shows the coordinate system.

A thermometer reading every 30 minutes served to register the water jet temperature. Variations of 2°F to 4°F were allowed between the beginning and end of each run.

No particular temperature control was used in the case of the jet of air, since the air was continuously resupplied from the room of experimentation.

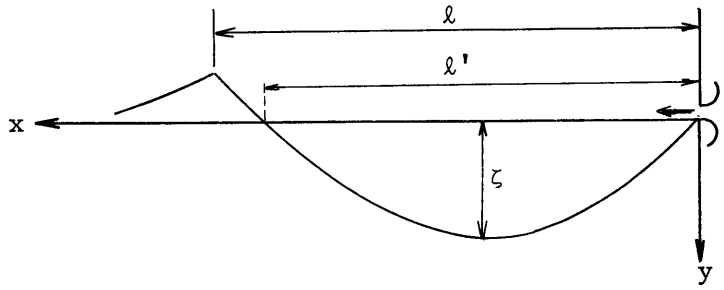

Fig. 17. Coordinate system to measure the scour profile

4.4. Description of the scour process

The air or water jets flowing over a bed of sand produce a shear effect on the uppermost grains, and put them in movement. The mode of sediment movement will depend on the magnitude of the lift force acting on the grains. The fact that the jet velocity decreases with the distance from the outlet section, in this case from the horizontal slot will explain the skewed form of the scour profiles observed at the beginning of the runs. Fig. 18(a) shows this initial scour geometry.

After a small scour hole is formed, the jet forms a separation zone within the hole and can entrain and mix with fluid from below. A recir-

culating movement in the form of an eddy is generated that produces a sediment movement against gravity forming a slope larger than the natural angle of repose of the sand, between the points B and O from Fig. 18(b). The sediment moves between these points mostly as bed load. This eddy acts from a stagnation point S, that is located in the position where the jet velocity begins to produce a higher shear stress in its own direction of movement. During a test, this point S changes position according to the jet oscillations. Downstream from this point, the sediment moves in suspension at the beginning of the test and as bed load after some vaguely defined time.

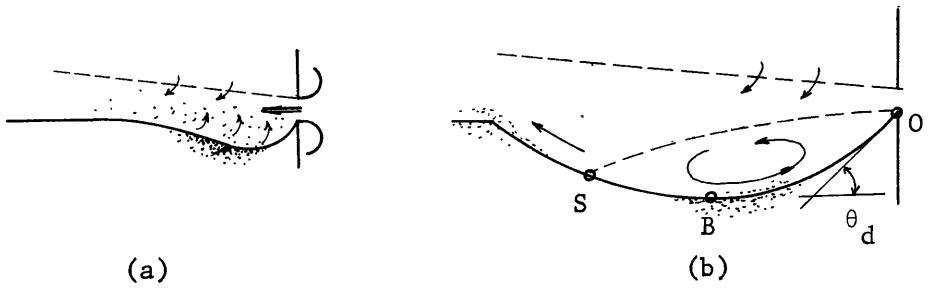

Fig. 18. Schematic representation of the scour hole formation

In the case of a jet of water, and after some distance from the origin, the shear stress is not high enough to keep the sediments moving as fast as the bottom eddy can scour the bed, and the sand begins to accumulate, deflecting the direction of the jet and forming a large, slowly rotating eddy over the upper boundary of the jet. As a consequence, downstream from the deposited sand, the water has only very reduced velocities; the sediment begins to deposit and shows essentially no movement after settling to the bed. See Fig. 19(a). The scour profile is

uniform throughout the transverse section of the second chamber of the experimental flume described in section 4.2.1. Only at the top of the deposited sediment and, far away from the jet origin, the transverse shape exhibits a variation in plan as shown in Fig. 19(b).

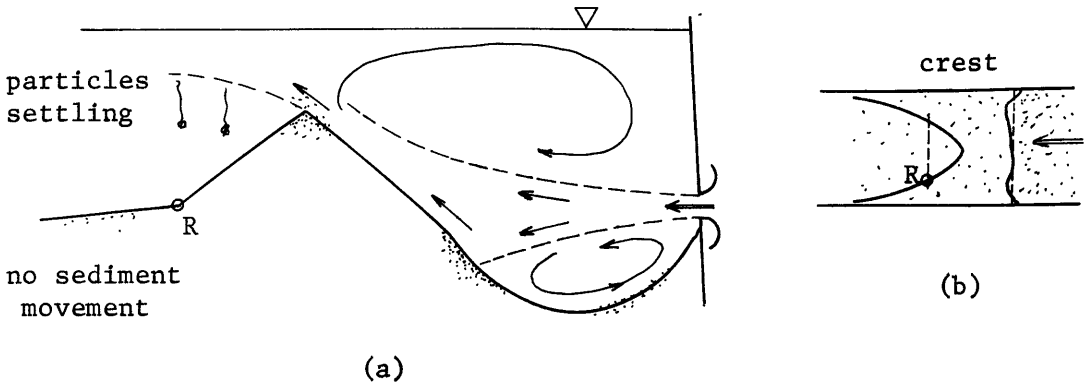

Fig. 19. Scour formation with a jet of water

For the case of a jet of air, as it was determined from experiments and described in section 3.1, the necessary shear stress due to the action of the flow of air to move the sediments is lower than in the case of water, and, consequently, the scour profile is larger than in the case of water under the same boundary conditions of jet discharge and sediment characteristics. Downstream from the scour hole, a small accumulation of sand with a very gentle slope is observed quite in contrast to the water conditions. The scour and profiles of deposition across the transverse section of the test chamber are very uniform, with only a slight excess rise near the top of the deposition in a very thin layer near the wall.

Since the test chamber was not covered, the air jet can be considered as discharging into an infinite medium with regard to the upper boundary and, consequently, no eddy is observed there.

Fig. 20 shows a characteristic progression of the scour hole. In the case of a jet of water, only cases (a) and (e) through (h) were observed.

4.5. Experimental results

Table 3 shows the different run conditions. A total of 16 experiments were carried out.

From the photographs, tables presenting four columns with data were prepared. The first two columns present the vertical and horizontal coordinates of the points of the scour profile. The third and fourth columns present the values of these coordinates normalized with respect to the length ℓ, as defined in sections 3.5 and 4.4. The entire set of photo-records and tables are kept on file at the Hydrodynamics Laboratory of M.I.T.

Appendix B presents a table with the summary of basic scour data and, as a sample, four photographs and their respective tables for each one of the scour patterns produced by the jet of water flowing with an initial mean velocity of 52 cm/s and by the jet of air flowing with an initial mean velocity of 17 m/s over a bed of sand 0.42 mm diameter.

Fig. 21 shows the similarity of the final or stable scour profiles for different ratios between U, the initial mean jet velocity and w, the particle mean fall velocity.

Fig. 22 shows an almost constant value of the ratios between ζ, the maximum depth of scour, and ℓ, the maximum length of scour, for different times of jet action, and different ratios U/w.

In the case of flow of the jet of air, the mean experimental value

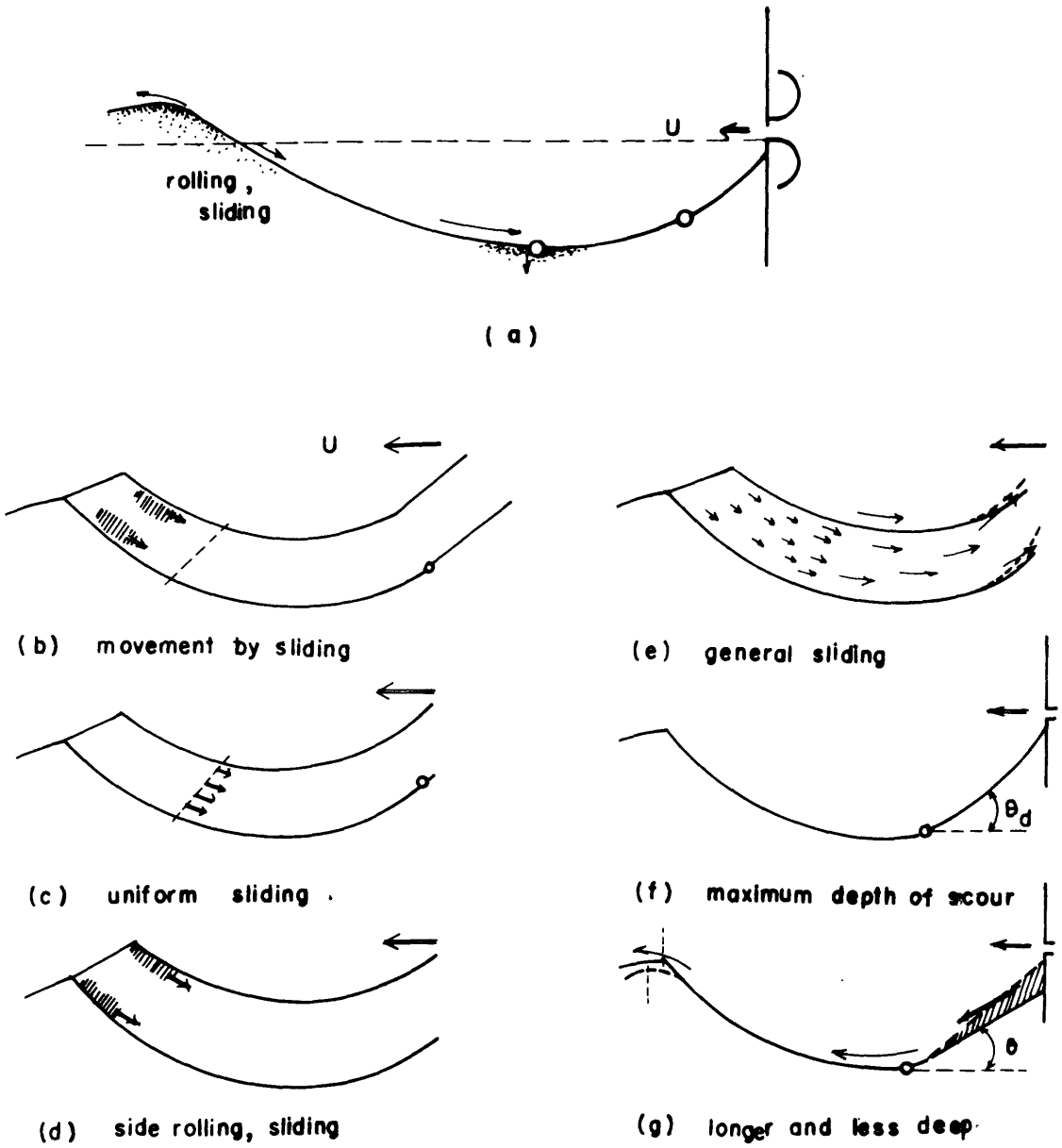

Fig. 20 Characteristic process of enlargement of the scour hole, by a jet of air

Table 3

Scour by jets of air and water. Experimental conditions.

d(mm)	Fall velocity · w(cm/s)			Jet velocity U(cm/s)		U/w			$(U/w)_r$	Test temperature °F	
	air (70°F)	water				air	water				
		59°	63°	air	water		59°	63°	63°	air	water
0.71	505	10.45	11.40	2020	40	4	3.83	3.51	1.140	73	60-63
				3030	60	6	5.74	5.26	1.141		58-62
0.59	450	9.54	9.57	900	32	2	3.35	3.34	0.599	72	62-64
				1800	48	4	5.03	5.02	0.797		62.5-65
				2700	64	6	6.71	6.69	0.897		62-65
0.42	315	6.72		1190	39	3.78	5.80		0.652	73	58-63
				1700	52	5.40	7.74		0.698		58-62
				2550	78	8.10	11.61		0.698		58.5-62

d (mm)	water	U/w	air	U/w
0.71	+	5.27	×	6
	▼	3.51	▽	4
0.59	↘	6.69	⊘	6
	↙	5.02	⌀	4
	●	3.34		
0.42	■	11.61	□	8.10
	▲	7.74	△	5.40
	◆	5.80	◇	3.78

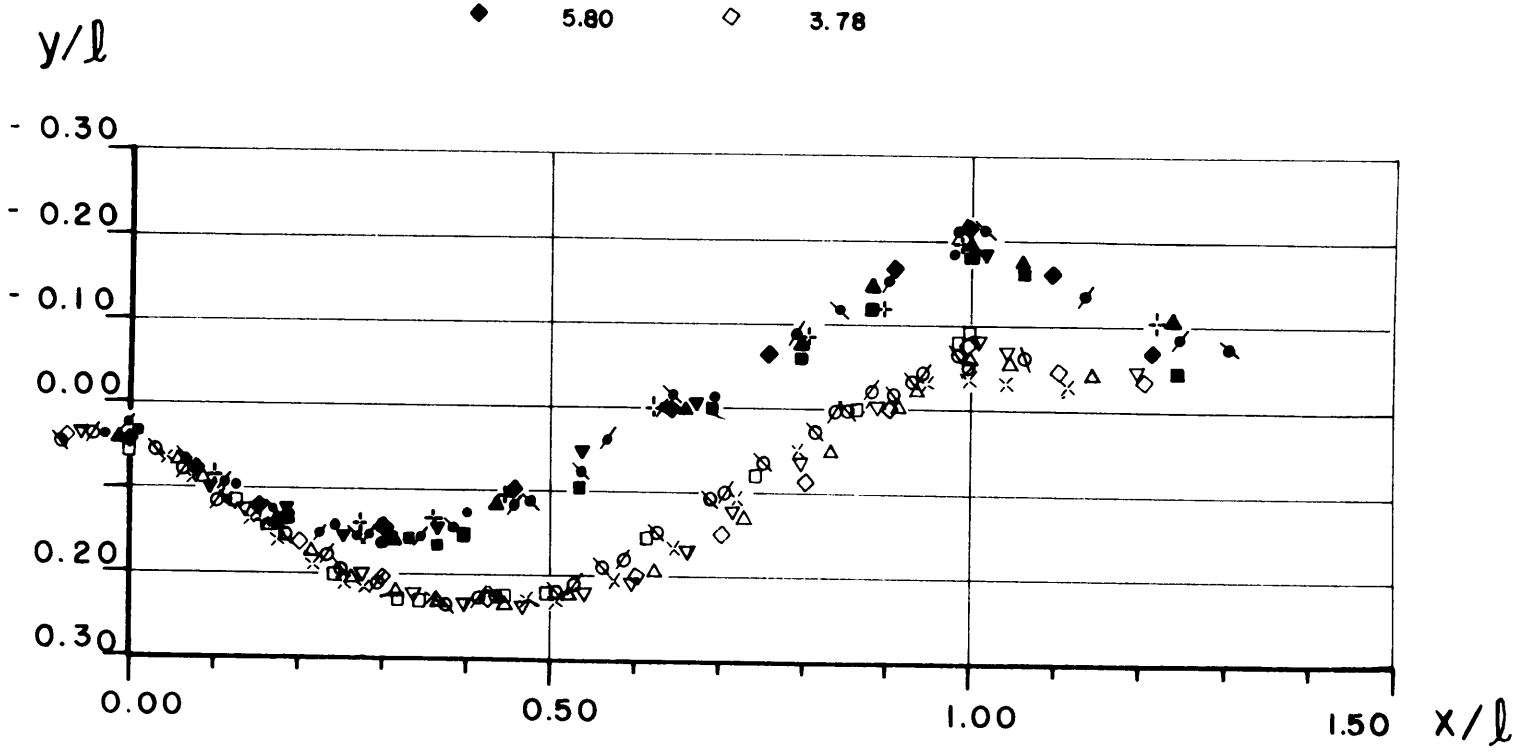

Fig. 21 Similarity of the stable scour profiles

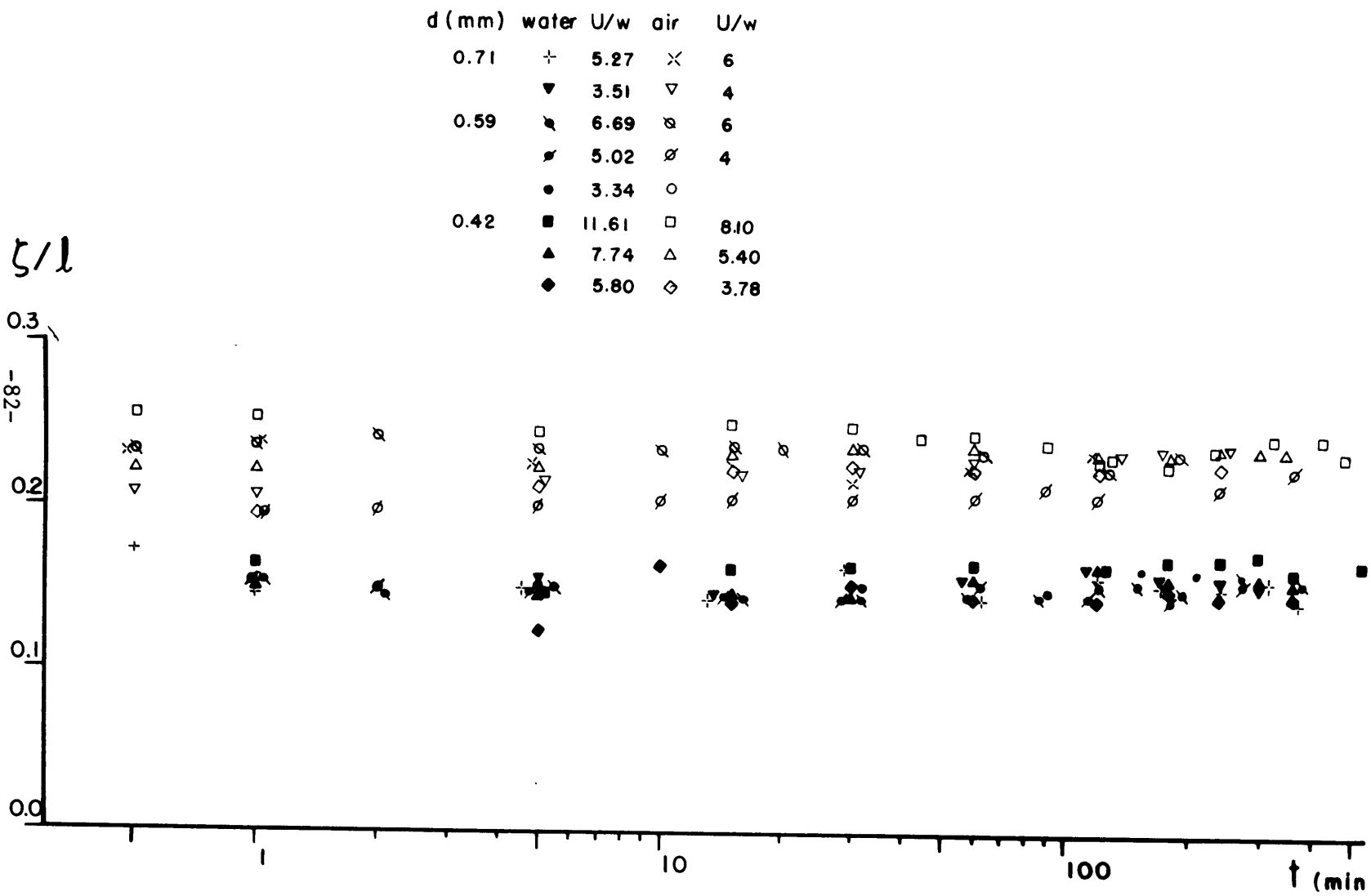

Fig. 22 Constancy of the normalized scour depth with time

(ζ/ℓ) air is equal to 0.225.

In the case of flow of the jet of water, the mean experimental value (ζ/ℓ) water is 0.154. And the ratio between the air and water maximum normalized depth of scour is

$$\left(\frac{\zeta}{\ell}\right)_r = \frac{(\zeta/\ell)_{air}}{(\zeta/\ell)_{water}} = \frac{0.225}{0.154} = 1.46$$

Table 4 and Fig. 23a show the influence of the ratio U/w, initial jet mean velocity to the particle mean fall velocity, in determining θ_d, the upstream slope of the scour profile. Higher values for this angle are observed in the case of action of a jet of air. Fig. 23(b) shows the relation existing between the normalized upstream slope θ_d with respect to the angle of repose θ and the ratio jet velocity to particle fall velocity for model and prototype.

4.6. Discussion

In order to clarify the experimental results, this discussion is divided in two parts; the first one will deal with the nature of the scour configuration for the two different fluids, and the second one will cover the validity of the proposed local scour parameters.

4.6.1. On the characteristics of the scour profiles by water and air currents

a) With the same experimental flume and sediments, and under similar ratios between the initial jet mean velocity and the particle mean fall velocity, the scour in the bed of sand is initially faster with air currents than with water currents. This fact seems to be a consequence of

Table 4

Upstream slope of the scour profile

Fluid	d(mm)	U/W		$(U/w)_r$	Upstream slope		Angle of repose		θ_d/θ	$(\theta_d/\theta)_r$
		59°	63°	63°	$\tan\theta_d$	θ_d	$\tan\theta$	θ		
Water	0.71	3.83	3.51		0.620	31°48'	.563	29°22'	1.083	
		5.74	5.26		0.650	33°01'			1.124	
	0.59	3.35	3.34		0.580	30°07'	.576	29°56'	1.019	
		5.03	5.02		0.625	32°			1.069	
		6.71	6.69		0.665	33°38'			1.124	
	0.42	5.80			0.610	31°23'	.588	30°43'	1.022	
		7.74			0.631	32°15'			1.050	
		11.61			0.646	32°52'			1.070	
Air	0.71	4		1.140	0.650	33°01'	.579	29°22'	1.12	0.956
		6		1.141	0.657	33°18'			1.13	1.005
	0.59	2		0.599	0.600	30°58'	.608	29°56'	1.035	1.016
		4		0.797	0.643	32°44'			1.094	1.023
		6		0.897	0.663	33°33'			1.121	0.997
	0.42	3.78		0.652	0.650	33°01'	.593	30°43'	1.077	1.054
		5.40		0.698	0.666	33°40'			1.098	1.046
		8.10		0.698	0.675	34°01'			1.109	1.036

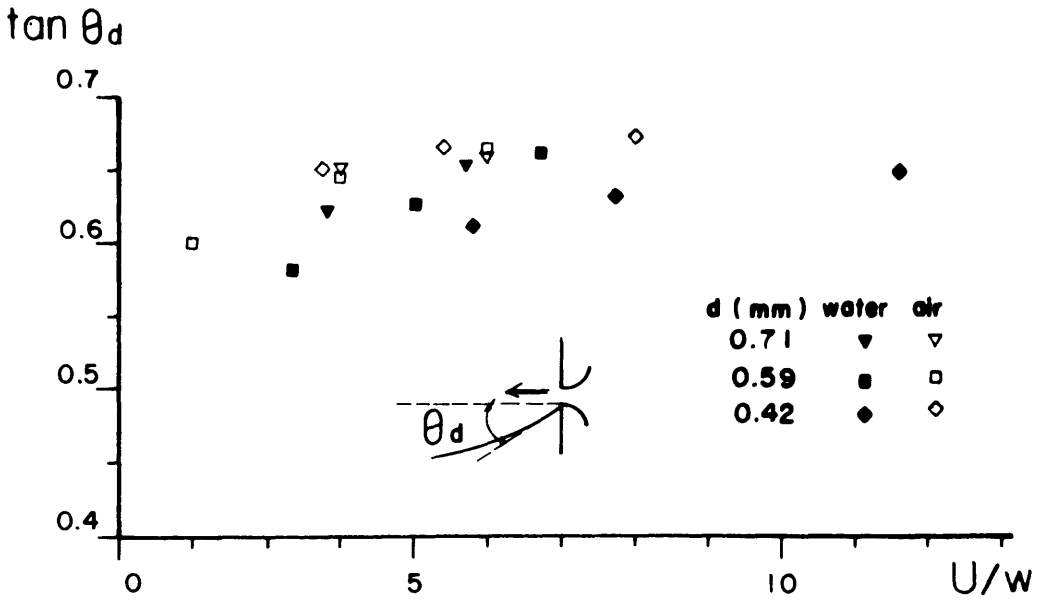

Fig. 23(a) Upstream slope of scouring hole θ_d vs. U/w

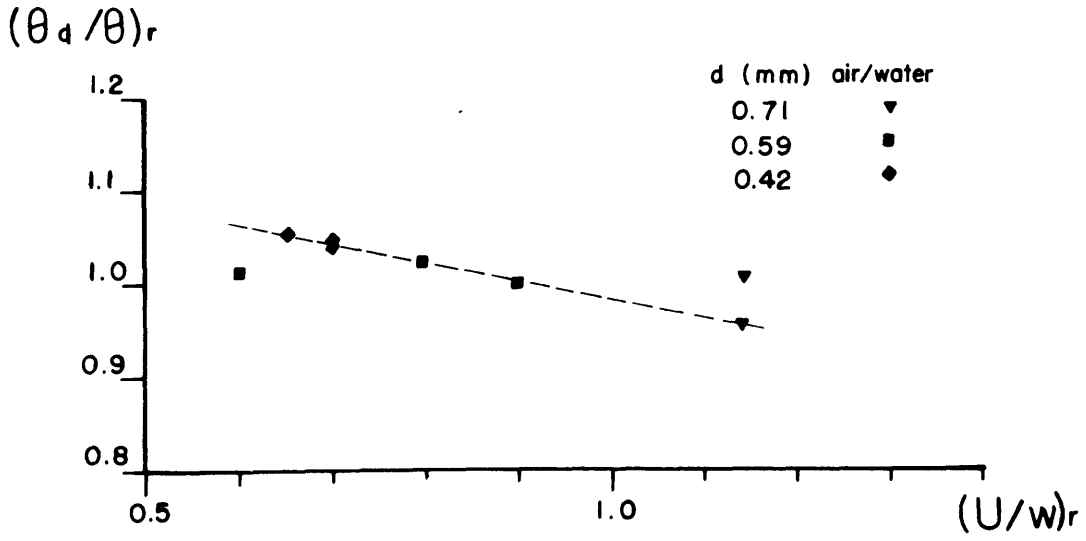

Fig. 23(b) Normalized upstream slope of scouring hole θ_d vs. U/w

the lower shear stress due to the flow necessary to move the sediments in air, as indicated for the proposed values of the Shields function, 0.056 in water and 0.0064 in air, see section 3.1.

b) After a scour hole is formed, from the stagnation point downstream, the sediment moves mostly in suspension in a small depth. From the stagnation point, toward the origin of the jet, the sediment movement is mostly as bed load and, in particular, by sliding and rolling, suggesting that the shear stress produced by the eddy, circulating below the jet, is lower than the shear stress produced from the stagnation point downstream by the jet itself. After some period of time the movement from the stagnation point downstream is also mostly as bed load.

c) The scour produced by a jet of air is deeper than the scour produced by a jet of water. Here, again, the difference between the necessary shear stress due to the different fluids plays a primary role.

d) The relative shapes of the scour, as can be deduced from photographs of the process, are rounded and proportional to each other, suggesting the possibility of modelling local scour by water currents using air currents in the laboratory.

e) Downstream from the scour hole, the water jet produces a deposition with a triangular form that is higher than the deposition of sediments generated by a jet of air. The origin of this difference is the lower value of the shear stress for air flow to move the sediments.

f) The accumulation of sediment in the case of the flow of the jet of water forces this jet to deflect, producing a large eddy between jet and free surface and reducing the velocities downstream of the deposition.

The particles, after crossing that crest, fall as in still water. In air, such a behavior is not observed. Instead, the transport of sediment, which moves with characteristic saltating trajectories, is predominant.

4.6.2. Validity of the parameters proposed to model local scour

The role of each one of the parameters proposed for a study of local scour will be independently analyzed in the following paragraphs.

a) Parameter U/w

The normalized stable profile of scour results essentially independent of the value of U/w within the range covered in the experiments, as can be seen in Fig. 21. During the experiments it was observed that after equilibrium in the mechanism of sediment movement inside the scour hole is reached, the normalized profiles of scour obtained with the jets of air and water are independent of the value of U/w and show a similar shape.

A variation in value of the ratio $(U/w)_r$ air-model to water-prototype from 0.599 to 1.141 was calculated for the present experiments as shown in Table 3. Therefore, the modelling of the local scour process by air and water jets can be assumed as valid at least for ratios $(U/w)_r$ close to unity.

Fig. 23a indicates the possible influence of the parameter U/w on the upstream slope of the scouring hole θ_d. A trend toward a constant value of θ_d is observed with increasing values U/w. Fig. 23b shows the relation between the values of θ_d normalized with respect to the angle of repose θ and values of U/w. However, it is to be noted that the upstream slope of the scouring hole θ_d does not vary much between the air

and water jets and different values of the ratio U/w.

b) Transient scour development

Fig. 22 shows that the normalized maximum scour depth is essentially independent of time.

The observed time to obtain the stable scour profiles with the jets of air and water were in the range of 6 hours and in a ratio of 1 to 1.2. Hence, the time scale for these experiments can be considered equal to one for air to water modelling of this type.

c) Parameter β_c/β

In the present laboratory study where the movement of sediment in the scour hole was mostly by rolling and sliding, the critical Shields function value should be the same in air and water and the ratio $(\beta_c/\beta)_r$ can be taken equal to unity.

d) Parameter $\frac{1}{t}\left(\frac{L}{g}\frac{\rho_s + k_2\,\rho_f}{\rho_s - \rho_f}\right)^{1/2}$

This parameter can be written in the form:

$$t\left(\frac{g}{L}\right)^{1/2}\left(\frac{\rho_s - \rho_f}{\rho_s + k_2\,\rho_f}\right)^{1/2}$$

Using the same experimental flume the scale of lengths is reduced to one, the time scale considered equal to one as confirmed by experiments, and the acceleration of gravity ratio equal to one, the ratio of the parameters for air and water reduces to:

$$\left(\frac{\rho_s - \rho_f}{\rho_s + k_2\,\rho_f}\right)_r^{1/2}$$

The shape of the sand used in the experiments was determined as

intermediate between a sphere and an ellipsoide with the aid of a microscope. The added mass coefficient in water can then be assumed equal to 0.35, an arithmetic average between k_2 = 0.5 the added mass coefficient for a sphere, and k_2 = 0.20 for an ellipsoide falling in the direction of its longer axis and with a ratio of 2:1 for the larger to the smaller axis.

Table 5 presents the values of the above parameter evaluated for added mass coefficients k_2 = 0.35 and 0.50 respectively. The added mass coefficients are of importance only for water, since the product $k_2 \rho_f$ becomes insignificant for air in comparison to ρ_s. In fact, the parameter reduces to the value of the above ratio for water.

Table 5

Values of $\left(\frac{\rho_s - \rho_f}{\rho_s + k_2 \rho_f} \right)_r^{1/2}$

d(mm)	Specific gravity	Values of parameter	
		k_2 = 0.35	k_2 = 0.50
0.71	2.73	1.46	1.54
.59	2.64	1.47	1.55
.42	2.67	1.463	1.55

Experimentally the value of the ratio, model to prototype, of the normalized maximum depth of scour was obtained equal to 1.46, see section 4.5. The applicability of the parameter for determining the depth normalized with respect to the length of scour with an added mass coefficient

in water equal to 0.35 is verified in the form:

$$\left(\frac{\zeta}{\ell}\right)_r = \left(\frac{\rho_s - \rho_f}{\rho_s + k_2 \rho_f}\right)_r^{1/2}$$

Table 6a shows the coordinates of the mean curves of the normalized measured scour profiles produced by the jets of water and air. Experimental results by Laursen (61) are also shown for his water tests. The results for air are reduced according to the value of the proposed parameter using both values of the added mass coefficient and are presented in Table 6b.

Fig. 24 shows fairly good agreement between the normalized scour profiles in water and the reduced normalized scour profile in air.

To further verify the applicability of the proposed parameter to model local scour, the present experiments in air are considered a model of the experiments carried on by Laursen (61) with a submerged jet of water issuing from a slot .025 ft. = .30 inches high.

Laursen does not present the specific gravity and the shape of the sand used in his experiments. The diameters with 50% of finer elements were used to check if the value of the fall velocity for quartz sand as it could be obtained using Fig. 8 taken from (40) coincide with the values of fall velocity as presented by Laursen. Since no significant differences were obtained between the fall velocities, it can be assumed that he used quartz sand in his experiments and hence the values of specific gravity, shape and added mass coefficients in water as used in the present experiments can be assumed as valid.

Table 6

Conformity between model and prototype measurements

Table a						Table b							
Water Measurement Experiments		Laursen Experim.		Air Experiments		Air Measurements Reduced by $(\rho_s-\rho_f/\rho_s+k_2\rho_f)_r^{1/2}$				Reduced by $\frac{1}{L_r^{1/2}}(\rho_s-\rho_f/\rho_s+k_2\rho_f)_r^{1/2}$			
						k = 0.35		k = 0.50		k = 0.35		k = 0.50	
x/ℓ	y/ℓ	x/ℓ	y/ℓ	x/ℓ	y/ℓ	x/ℓ	y/ℓ	x/ℓ	y/ℓ	x/ℓ	y/ℓ	x/ℓ	y/ℓ
0	.035												
.10	.095	.10	.085	.10	.11	.068	.075	.065	.071	.074	.082	.071	.078
.20	.135	.20	.138	.20	.17	.137	.116	.130	.110	.150	.127	.142	.120
.28	.151												
.30	.158	.30	.175	.30	.22	.205	.151	.195	.142	.224	.165	.214	.155
.40	.130	.40	.163	.40	.23	.274	.158	.260	.149	.300	.173	.285	.163
.50	.078	.50	.10	.50	.22	.342	.151	.325	.142	.374	.165	.356	.155
.635	0	.60	.038	.60	.18	.411	.123	.390	.117	.450	.135	.427	.128
		.663	0	.70	.12	.479	.082	.455	.078	.525	.090	.498	.085
.80	-.091	.80	-.095	.80	.055	.548	.038	.519	.036	.600	.042	.568	.039
.90	-.14	.90	-.14	.875	0	.599	0	.568	0	.656	0	.622	0
1.	-.205	1	-.20	1	-.08	.685	.055	.649	.052	.750	.060	.711	.057
1.2	-.10	1.2	-.05	1.1	-.05	.753	.034	.714	.032	.825	.037	.782	.035
				1.2	-.04	.822	.027	.778	.026	.900	.030	.853	.028

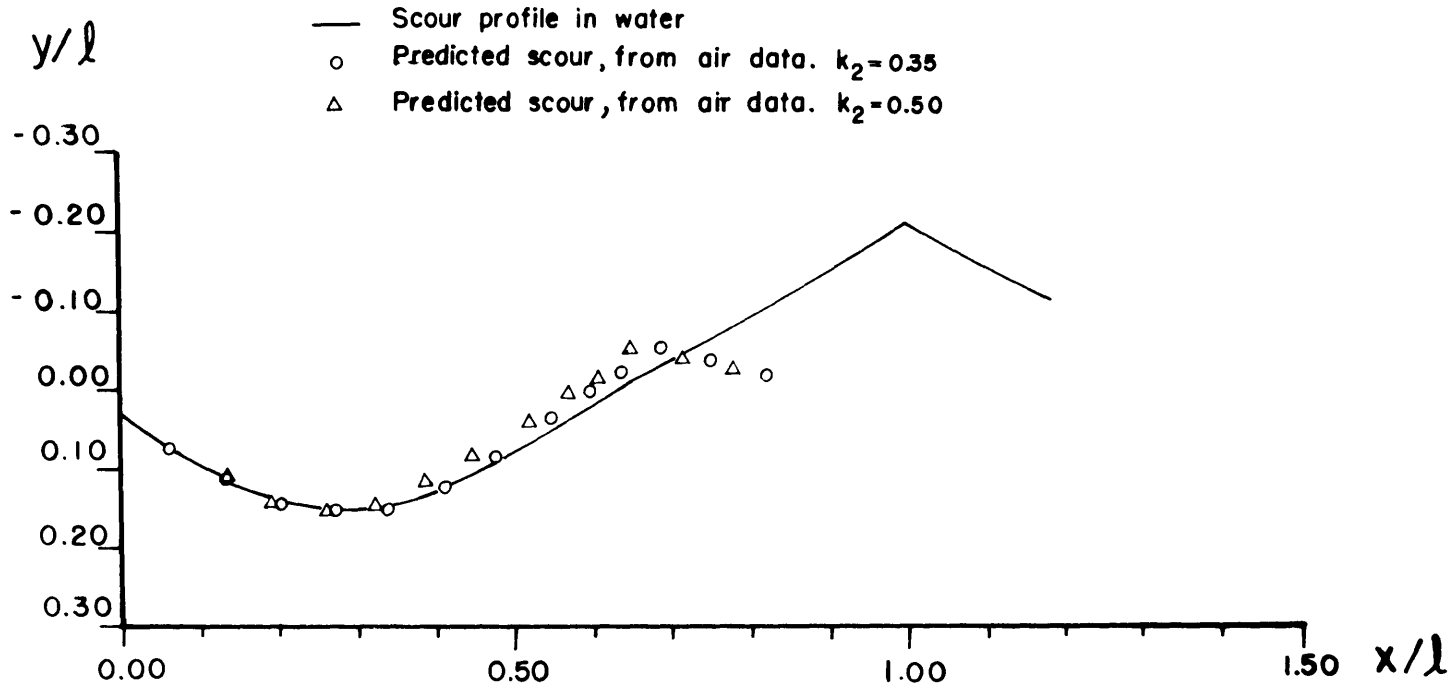

Fig. 24 Comparison between normalized scour in water and predicted scour based on air data

It remains only to correct the value of the parameter, as presented in Table 5, by the length scale. The length scale is equal to the ratio between the heights of the issuing jets, since they are the significant lengths in this two-dimensional problem.

$$L_r = \frac{y_{o\ m}}{y_{o\ p}} = \frac{0.25 \text{ in}}{0.025 \text{ ft} \times 12 \text{ in/ft}} = \frac{1}{1.2}$$

Table 6b also presents the values of the scour profile measured in air reduced by the factor

$$\frac{1}{L_r^{1/2}} \left(\frac{\rho_s - \rho_f}{\rho_s + k_2 \rho_f} \right)_r^{1/2}$$

using added mass coefficients in water of 0.35 and 0.50.

The agreement between the Laursen results in water, the normalized scour profiles of the present experiments in water and the scour profile based on air data is notable. This can be seen graphically on Fig. 25 for an added mass coefficient in water of .35, verifying the applicability of the proposed parameter.

It may be noted further that the Laursen experiments in water were carried out with U/w ratios as high as 32, while the present water tests did not have values higher than 11.6 for this ratio.

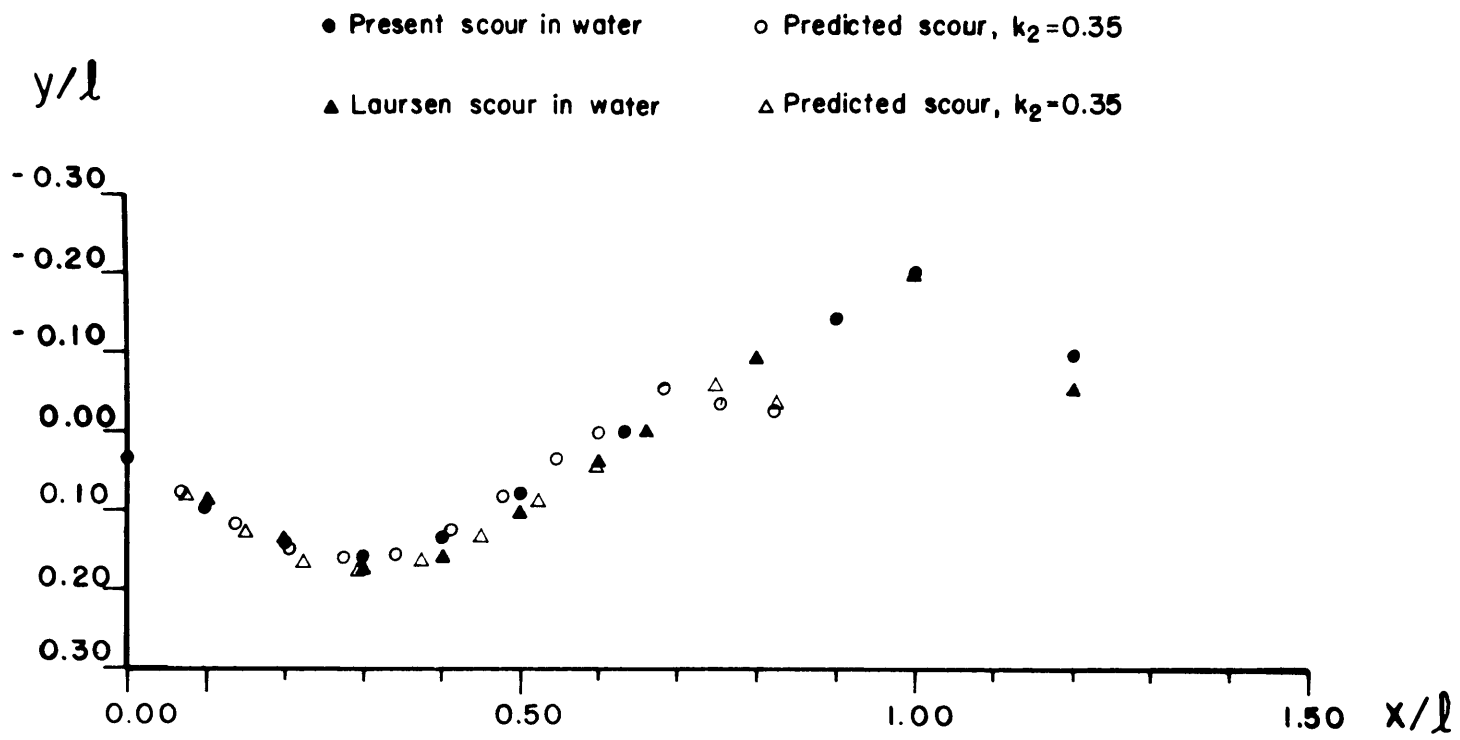

Fig. 25 Conformity between the present experiment and Laursen scour in water and their prediction based on air data

V. CONCLUSIONS

The experiments reported in this study and their similarity analysis permit the following general conclusions.

1. Air jets can be used to model the scour produced by water currents over an initially horizontal flat bed of sand. The similarity parameters proposed in this study to model such local scour are verified.

2. Within the scour holes produced by the water and air currents, the sand moves in the same mode, mostly by rolling and sliding. However, at the beginning of the development of the scour hole the sand moves in suspension and in saltating patterns downstream of a certain point.

3. Downstream of the scour hole the sand is deposited in different patterns for air and water. For water jets a fairly well defined triangular dune is formed above the original bed elevation which is considerably higher than the deposit formed downstream of the scour hole for air. For water, all sand movement downstream of the dune is stopped as a consequence of the jet deflection upwards. For air, characteristic transport by saltation continues for a considerable distance, so that the deposit remains low and relatively flat.

4. With the acceleration of gravity and time scales equal to unity, the scale ratio of the normalized depth of scour is given by:

$$\left(\frac{\zeta}{\ell}\right)_r = \frac{1}{L_r^{1/2}} \left(\frac{\rho_s - \rho_f}{\rho_s + k_2 \rho_f}\right)_r^{1/2}$$

5. The normalized scour profiles produced by the air and water jets remain essentially constant with time, i.e. the profiles obtained at successive intervals of time are similar.
6. The ratio for the periods necessary to obtain stable scour profiles by air and water jets was found essentially equal to unity.
7. The ratio between the initial jet mean velocity to the particle mean fall velocity $(U/w)_r$ can assume any value.
8. In air as well as in water, larger ratios U/w, give larger values of the upstream slope of the scour hole, although this angle shows only a very small variation.
9. In short, with velocities higher than critical for sediment transport for air jets and water jets this particular study established that geometric similarity can be achieved independent of the dynamic factors and sediment properties.

VI. RECOMMENDATIONS

1. Parameters for modelling local scour.

   a. It is suggested that laboratory tests with jets of air and water be carried out using different density ratios and different added mass coefficients in water by experimenting, i.e., with spherical or cylindrical plastic beads.

   b. A wind tunnel should be used to explore the applicability of the modelling parameter for three-dimensional problems of scour, i.e., produced by currents of water crossing bridge piers or expansions of the transverse section of flow.

2. Parameters for modelling bed load and suspended load.

Air currents should be used to explore the applicability of the parameters proposed to model the bed and suspended load of natural streams of water.

REFERENCES

1. Shields, A., "Anwendung der Aehnlichkeitsmechanick und der Turbulenzforschung auf die Geschiebebewegung", Mitteilungen der Preussischen Versuchsanstalt fur Wasserbau und Schiffbau, Berlin, 1936. English translation by Ott, W. and vanUchelen, J., Soil Conser. Service Coop. Lab., California Inst. of Technology, Pasadena, California.
2. Einstein, H., Chien, N., "Similarity of distorted models with movable beds", Transactions ASCE, Paper 2805, 1956, pp. 440-462.
3. Gukhman, A., "Introduction to the theory of similarity", Academic Press, New York, 1965. (Translated from the Russian Ed. 1963).
4. Langhaar, H., "Dimensional analysis and theory of models", John Wiley & Sons Inc., New York, 1951.
5. Murphy, G., "Similitude in Engineering", The Ronald Press Co., New York, 1950.
6. Sedov, L., "Similarity and Dimensional Methods in Mechanics", Academic Press, New York, 1959. (Translated from the Russian 4th ed.).
7. Skoglund, V., "Similitude: Theory and Applications", International Textbook Co., Penn., 1967.
8. ASCE, Hyd. Div., "Hydraulic Models", Manual no. 25, 1942.
9. Warnock, J., "Hydraulic Similitude", Chapter II. Eng. Hydraulics, edited by Rouse, H., John Wiley, New York, 1949.
10. Allen, J., "Scale Models in Hydraulic Engineering", Longmans Green & Co., London, 1947.

11. Foster, J., "Fixed Bed River Models", ASCE, Washington Convention, October 1959.

12. Lab. Nacional de Hidraúlica, "Estudio en modelo hidraúlico de la bocatoma del Proj. de Irrig. de Chao y Virú", Inf. técnico 3-007, Lima, Perú, May 1966.

13. Lab. Nacional de Hidraúlica, "Estudio en modelo hidraúlico de la remodelación de la bocatoma de la Puntilla", Inf. técnico 3-012, Lima, Perú, Julio 1967.

14. Du Boys, P., "Etudes du régime du Rhône et l'action exerceé par les eaux sur un lit à fond de graviers in definiment affouillable", Annales des Ponts et Chausseés, Ser. 5, 18, 1879, pp. 141-195.

15. Schoklitsch, A., "Arquitectura Hidraúlica", Gustavo Gili, Barcelona, 1946.

16. Kalinske, A., "Movement of sediment as bed in rivers", Trans. Am. Geophysics Union 28, 1947, pp. 615-620.

17. Meyer-Peter, E. and Müller, R., "Formulae for bed load transport", Proc. 2nd Meeting, IAHR, Stockholm, June 7-9, 1948, pp. 39-64.

18. Einstein, H., "The bedload function for sediment transportation in open channel flows", U.S. Dept. of Agriculture, Tech. Bulletin no. 1026, Washington, D.C., September 1950.

19. Blench, T., "Regime theory for self-formed sediment bearing channels" with discussions by Laursen, E., Matthes, G., and Blench, T., Trans. ASCE, vol. 117, 1952, pp. 383-408.

20. Yalin, S., "An expression for bed load transportation", Proc. ASCE, HY3, Paper 3525, May 1963, pp. 221-250.

21. Bagnold, R. A., "The Physics of Blown Sand and Desert Dunes", Methuen & Co. Ltd., London, 1941. (Reprint 1960).

22. Kawamura, R., "Study of sand movement by wind", Transl. from Japanese, Hyd. Eng. Lab. Wave Research Projects, Univ. of California, Berkeley, June 1964.

23. Kadib, A., "A function for sand movement by wind", Hyd. Eng. Lab. Wave Research Projects, Univ. of California, Berkeley, January 1965.

24. Chiu, T. Y., "Sand transport by wind", Department of Coastal and Oceanographic Eng., College of Eng., Univ. of Florida, Gainesville, Florida, Tech. Report no. 1.

25. Blench, T., "Scale relations among sand-bed rivers including models", Proc. ASCE, vol. 81, separate 667, Hy. Div., April 1955.

26. Einstein, H., Disc. of "Scale relations among sand-bed rivers including models" by Blench, T. (Proc. paper 667, ASCE, 1955). Proc. ASCE, separate 794, vol. 81, Hy. Div., 1955.

27. Colby, B. and Hembree, C., "Computations of total sediment discharge Niobrara River near Cody, Nebraska", Geological Survey Water Supply paper no. 1357.

28. U.S. Bureau of Reclamation, "Step method for computing total sediment load by the modified Einstein procedure", Denver, Colorado, July 1955.

29. Vanoni, V. and Brooks, N., "Laboratory studies of the roughness and suspended load of alluvial streams", Sedimentation Lab., California Inst. of Tech., Pasadena, California, Report No. E-68, December 1957.

30. Bogardi, J., "Hydraulic similarity of river models with movable bed",

Acta Technica, Academiae Scientiarum Hungaricae, Tomus XXIV, Fasciculi 3-4, 1959, pp. 417, 446.

31. Rouse, H., "Criteria for similarity in the transportation of sediment", Proc. Hyd. Conference, Univ. of Iowa Studies in Eng., Bulletin 20, 1940, pp. 33-49.

32. Yalin, S., "Similarity in sediment transport by currents", Ministry of Technology, Hydraulic Research Station, Paper no. 6, London, Her Majesty's Stationary Office, 1965.

33. Field, W., "Effects of density ratio on sedimentary similitude", Proc. ASCE, HY3, Paper 5948, May 1968, pp. 705-719.

34. Barr,D. and Herbertson, J., "Similitude theory applied to correlation of flume sediment transport data", Water Resources Research, vol. 4, no. 2, April 1968, pp. 307-315.

35. Gradowczyk, M. and Folguera, H., "Analysis of scour in open channels by means of mathematical models", Instituto de Cálculo, Fac. de Ciencias Exactas y Naturales, Univ. de Buenos Aires, Publication no. 6, Buenos Aires, Argentina, March 1965.

36. Bagnold, R., "The flow of cohesionless grain in fluids", Philosophical Trans. of the Royal Soc. of London, Ser. A, Math. and Physical Sciences, No. 964, vol. 249, December 1956, pp. 235-297.

37. Zingg, A., "Wind tunnel studies of the movement of sedimentary materials", Bulletin 34, Proc. of the 5th Hydraulics Conf., Iowa Institute of Hyd., Iowa City, 1953, pp. 111-135.

38. Chepil, W., "Dynamics of wind erosion: II. Initiation of soil movement", Soil Science 60, 1945 a, pp. 397-411.

39. Jeffreys, H., "On the transport of sediments by streams", Cambridge Philosophical Society, Proc. V25, 1929, pp. 272-276.

40. ASCE Comm. on Preparation of Sedimentation Manual, Sediment Transport Mechanics, "Introduction and properties of sediments", Proc. paper 3194, HY4, July 1962, pp. 77-107.

41. ASCE Comm. on Preparation of Sedimentation Manual, Sediment Transport Mechanics, "Initiation of motion", Proc. paper 4738, HY2, March 1966, pp. 291-314.

42. White, C., "The equilibrium of grains on the bed of a stream, Royal Soc. of London, Proc. Ser. A, vol. 174, 1940, pp. 322-338.

43. Carstens, M., Neilson, F., Altinbilek, H., "Bed forms generated in the laboratory under an oscillatory flow: Analytical and experimental study", TM-28, U.S. Army Corps of Eng. Coastal Eng. Research Center, June 1969.

44. Vanoni, V., "Data used to develop Shields diagram", Mem. 65.2, Calif. Inst. of Tech., W. M. Keck Lab. of Hydraulics and Water Resources, April 1965.

45. Ippen, A., Verma, R., "The motion of discrete particles along the bed of a turbulent stream", Proc. Minnesota International Hyd. Convention, Minneapolis, Minnesota, September 1-4, 1953, pp. 7-20.

46. Ward, B., "Relative density effects on incipient bed movement", Water Resources Research, vol. 5, no. 5, October 1969, pp. 1090-1096.

47. Sutherland, A., "Proposed mechanism for sediment entrainment by turbulent flows", Journal of Geophysical Research, December 15, 1967, vol. 72, no. 24, pp. 6183-6194.

48. Bagnold, R., "An approach to the sediment transport problem from General Physics", Geological Survey Prof. paper 422-I, U.S. Govern. Print., Washington, 1966.

49. Owen, P., "Saltation of uniform grains in air", J. Fluid Mechanics, vol. 20, part 2, 1964, pp. 225-242.

50. Nordin, C., Beverage, J., Discussion of "An expression for bed load transportation" by Yalin, S., ASCE Proc. HY1, January 1964, pp. 303-313.

51. Vanoni, V., "Transportation of suspended sediment by water", Trans. ASCE, vol. 111, 1946, pp. 67-133.

52. Ismail, H., "Turbulent transfer mechanism and suspended sediment in closed channels", Trans. ASCE, vol. 117, 1952, pp. 409-446.

53. Carstens, M., "Accelerated motion of a spherical particle", Trans. American Geophysical Union, vol. 33, no. 5, 1952, pp. 713-720.

54. McNown, Pin Nam Lin, "Sediment concentration and fall velocity", Proc. 2nd Midwestern Conference on Fluid Mechanics, Ohio State Univ., Columbus, Ohio, 1952, pp. 401-411.

55. Coronado, F., "Pruebas de sedimentación en agua tranquila de arenas del río Mantaro", Inf. técnico 3-010, Lab. Nac. de Hidraúlica, Lima, Perú, October 1966.

56. O'Brien, "Review of the theory of turbulent flow and its relation to sediment transportation", Trans. Amer. Geophysical Union, April 1933, pp. 487-491.

57. ASCE, Task force on friction factors in open channels of Comm. on Hydromechanics, "Friction factors in open channels", Proc. paper

3464. HY2, March 1963, pp. 97-143.

58. Alam, A., Cheyer, T., Kennedy, J., "Friction factors for flow in sand bed channels", MIT Hydrodynamics Lab. Report no. 78, June 1966.

59. Lovera, F., Kennedy, J., "Friction factors for flat-bed forms in sand channels", ASCE Proc. paper 6678, HY4, July 1969, pp. 1227-1234.

60. Herbertson, J., Discussion of "Alluvial channel resistance related to bed form" by Kenneth Smith, Proc. ASCE, HY1, January 1969, pp. 473-475.

61. Laursen, E., "Observations on the nature of scour", Iowa Inst. of Hydraulics Research, Bulletin 36, 1952, pp. 179-197.

62. Laursen, E., "Scour at bridge crossings", with disc. by Blench, Bradley, Joglekar, Bauer, Tison, Chitale, Thomas, Mushtag, and Romita L., Trans. ASCE, paper 3294, vol. 127, part I, 1962, pp. 166-180.

63. Laursen, E., "An analysis of relief bridge scour", ASCE Proc. paper, HY3, May 1963, pp. 93-118.

64. Carstens, M., "Similarity laws for localized scour", ASCE Proc. paper 4818, HY3, May 1966, pp. 13-36.

65. Yalin, S., "Geometrical properties of sand waves", ASCE Proc. paper, HY5, 1964, pp. 105-119.

66. Nordin, C., "Aspects of flow resistance on sediment transport, Rio Grande near Bernalillo, New Mexico", Water Supply paper 1498-H, U.S. Geological Survey, 1964.

APPENDIX A

LIST OF SYMBOLS

a	distance over the sediment bed level
b	channel or river width
c	concentration of sediments at a point and time
d	sediment nominal diameter
d_o	mean size of a standard sand taken as 0.25 mm
e	dimensional coefficient for rate of sediment transported by air
f	expressing function, Darcy friction factor
f'	grain friction factor in Darcy friction formula
f''	bed form friction factor in Darcy friction formula
g	acceleration of gravity
h	maximum height reached by sediments on saltation
j	exponent of the fluid discharge for the regime theory formulae
k	coefficients
k_1	shape factor of sediments
k_2	added mass coefficient
k_e	height roughness
ℓ	characteristic length of a localized scour
m	virtual mass
m_s	mass of sediment
n	Manning formula's coefficient
p	exponent for the rate of sediment transported by air
q	fluid discharge per unit width

q_s	sediment discharge rate per unit width
r	as subindex, ratio between model and prototype values
t	time
u	flow velocity component along the channel flow
u_c	threshold velocity along the channel flow
u_*	shear velocity
u_{*c}	critical shear velocity
v	vertical component of the flow velocity
w	sediment settling velocity, and lateral component of flow velocity
x, y, z	longitudinal, vertical and lateral coordinate axis respectively with origin over the mean bed level
y_o	mean flow depth
A	sediment projected section normal to the lift force
B_s	Bagnold initiation of suspension parameter
C	reference value of concentration
C_a	sediment concentration at a level "a"
C'_D	drag coefficient
C'_L	lift coefficient
C_2, C_3	two and three-dimensional concentration respectively
D	drag force on a sediment
D(s)	drag force along the sediment trajectory
D(y), D(x)	vertical and longitudinal projections of drag force
E	turbulent diffusion coefficient per mass
E_m	turbulent diffusion coefficient per momentum

G	defined as equal to $\left(\frac{\rho_s - \rho_f}{\rho_s + k_2 \rho_f}\right)g$
K_1, K_2	coefficient function of the shear Reynolds number
L	lift force at a height y over the bed
L_o	lift force on the bed
L_{oc}	critical lift force on the bed
M	defined as equal to u_*^2/u_{*c}^2
Q	fluid discharge
Q_s	sediment discharge
R	hydraulic radius
S_o	bed slope
S_f	gradient of the energy
T	time scale
U	velocity scale
W	sediment submerged weight
$(\ )^\circ$	dimensionless quantity
$(\ )_p$, $(\ )_m$	prototype and model values
α	coefficient giving the form of variation of the lift force with height
β	Shields' function
β_c	Shields' critical function
δ	laminar sublayer thickness
ξ	local scour depth
θ	sediments angle of internal friction
θ_d	angle of the upstream slope of a scouring hole

ϕ	bed angle of inclination with respect to the x direction
η	dimensionless depth equal to y/d
η_o	dimensionless depth equal to y/y_o
λ	ratio between the turbulent diffusion coefficient per momentum and per mass
ν	fluid kinematic viscosity
ρ_s, ρ_f	sediment and fluid densities
σ_s, σ_w	standard deviation of sediment sizes, and fall velocities
τ_o	bed shear stress
τ_B	shear stresses at the lowest point of a local scour
τ_c	critical shear stress
τ_s, τ_w	impact and horizontal shear stresses
Ψ_*, Φ	Einstein's intensity shear and transport parameters

APPENDIX B

CHARACTERISTIC PHOTOGRAPHS AND TABLES SHOWING THE SCOUR

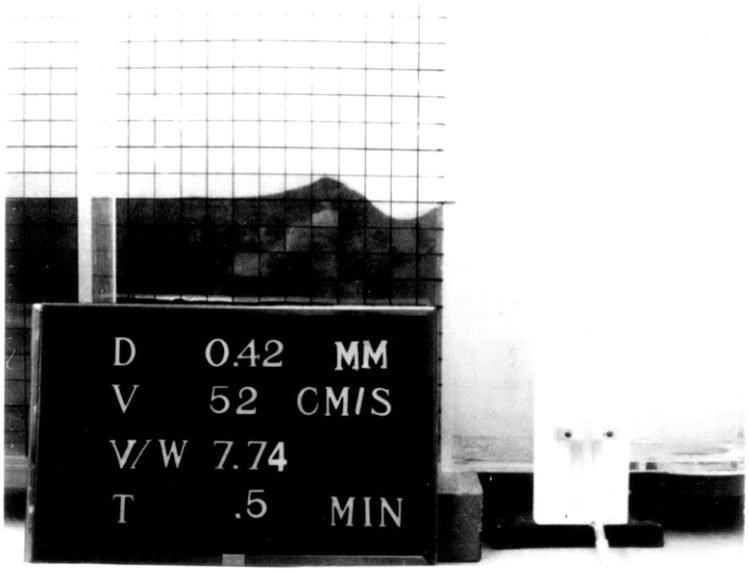

Photo 6. Water jet scour, d = 0.42 mm, U/w = 7.74

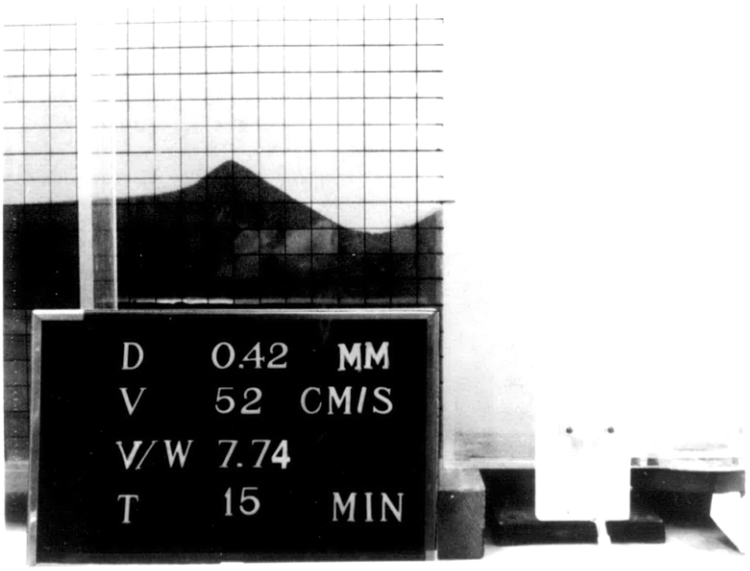

Photo 7. Water jet scour, d = 0.42 mm, U/w = 7.74

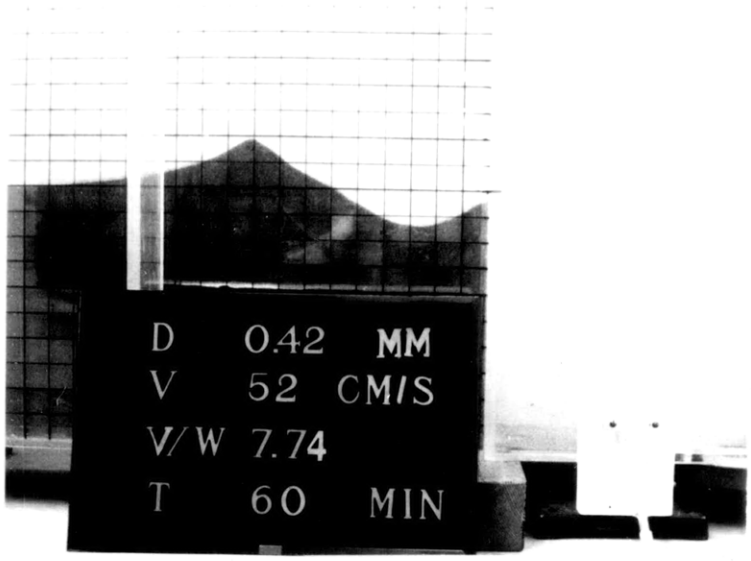

Photo 8. Water jet scour, d = 0.42 mm, U/w = 7.74

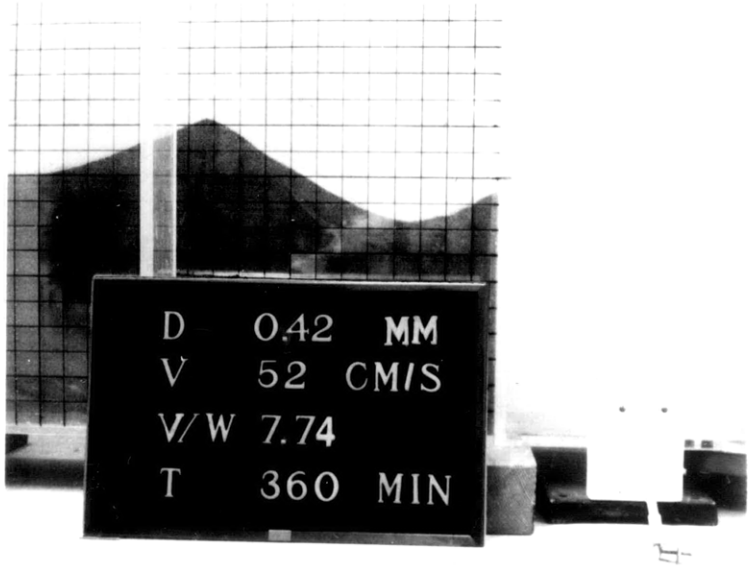

Photo 9. Water jet scour, d = 0.42 mm, U/w = 7.74

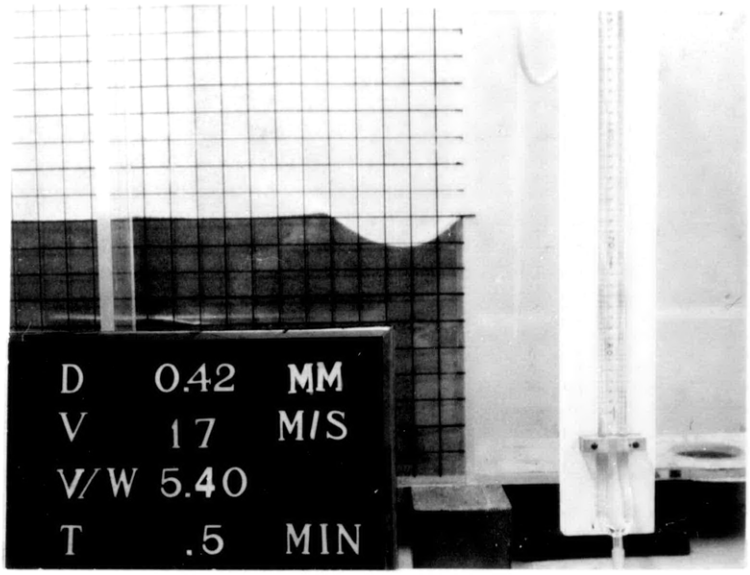

Photo 10. Air jet scour, d = 0.42 mm, U/w = 5.40

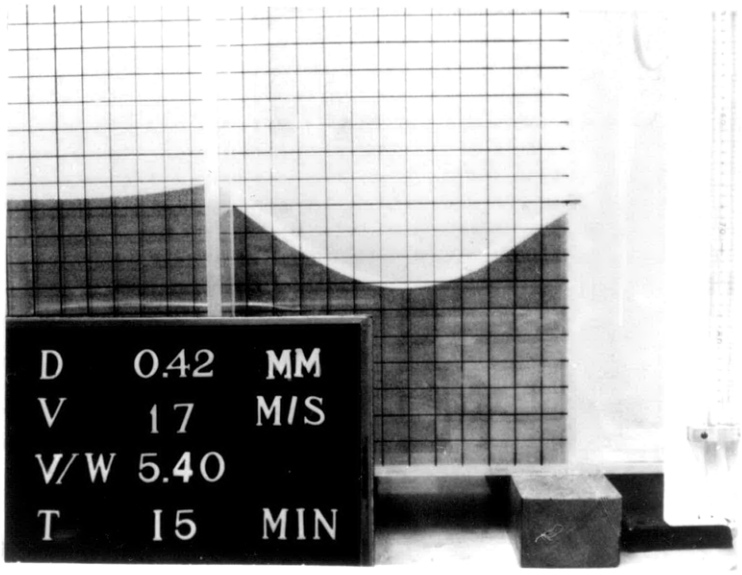

Photo 11. Air jet scour, d = 0.42 mm, U/w = 5.40

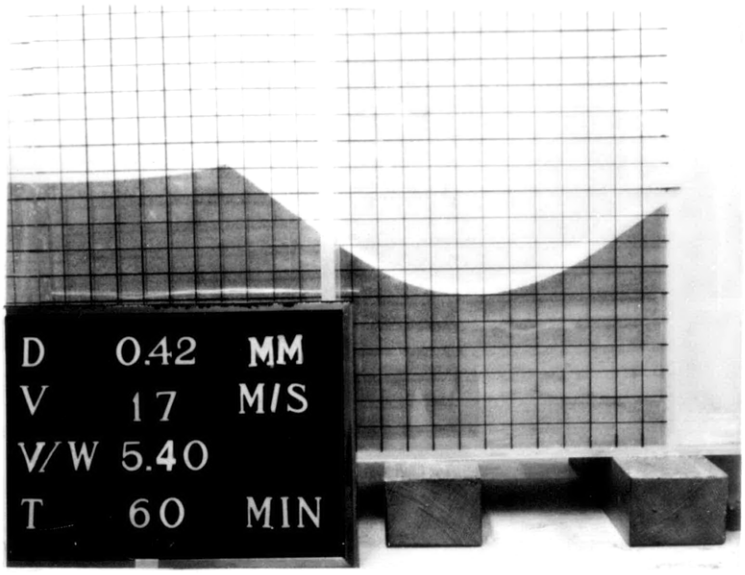

Photo 12. Air jet scour, d = 0.42 mm
U = 17 cm/s U/w = 5.40

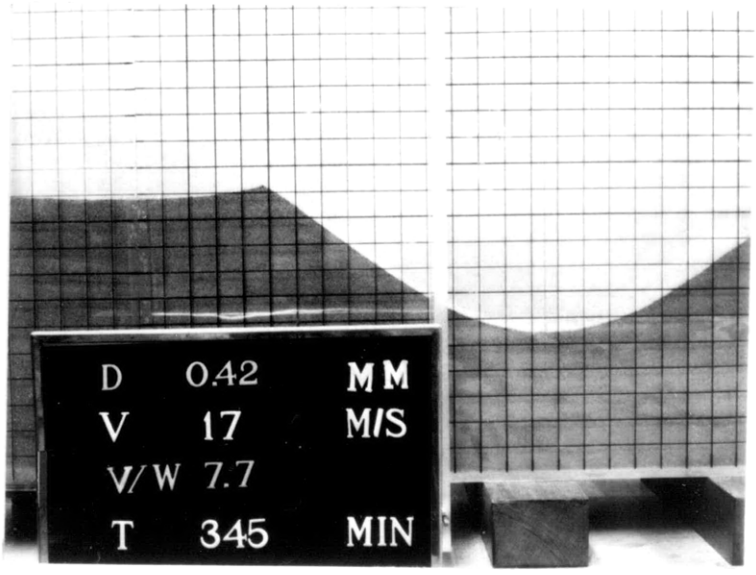

Photo 13. Air jet scour, d = 0.42 mm
U = 17 cm/s U/w = 5.40

Table 7

Jet of water. Scour profiles.

d = 0.42 mm U = 52 cm/s w = 6.72 cm/s U/w = 7.74

t = 0.5 min

x	y	x/ℓ	y/ℓ
0	0	-	-
1	0.60	.182	.109
1.5	0.70	.273	.127
2	0.60	.364	.109
2.83	0	.515	0
4.1	-0.16	.745	-.029
5.5	-0.92	1	-.167
6	-0.60	1.091	-.109
7	-0.33	1.273	-.060
8	-0.10	1.455	-.018

t = 60 min

x	y	x/ℓ	y/ℓ
0	0.33	0	.037
0.33	0.46	.037	.051
2	1.30	.222	.144
2.50	1.42	.278	.158
3	1.33	.333	.148
4	1.10	.444	.122
6	0	.667	0
7.70	-1.0	.855	-.111
9	-1.88	1	-.209
11	-1.0	1.222	-.111
13	-0.25	1.444	-.028
15	0	1.667	0

t = 15 min

x	y	x/ℓ	y/ℓ
0	0.20	0	.025
1.12	0.92	.137	.113
1.42	0.92	.174	.113
2	1.10	.245	.135
2.5	1.20	.306	.147
3	1.12	.368	.137
4	0.85	.490	.104
5.33	0	.653	0
7	-1.0	.858	-.123
8.16	-1.66	1	-.203
9.40	-0.75	1.152	-.092
11	-0.30	1.348	-.037
14	0	1.716	0

t = 360 min

x	y	x/ℓ	y/ℓ
0	0.45	0	.040
1	1.0	.088	.088
2	1.50	.177	.133
2.40	1.50	.212	.133
3.40	1.75	.301	.155
4	1.66	.354	.147
5	1.33	.442	.118
7.5	0	.664	0
9	-0.85	.796	-.075
10	-1.65	.885	-.146
11.30	-2.20	1	-.195
12	-2.0	1.062	-.177
14	-1.25	1.239	-.111
16	-0.50	1.416	-.044
18	0	1.593	0

Table 8

Jet of air. Scour profiles.

d = 0.42 mm U = 1700 cm/s w = 315 cm/s U/w = 5.40

t = 5 min

x	y	x/ℓ	y/ℓ
0	0	-	-
1	0.78	.190	.149
1.5	1	.286	.190
2.25	1.16	.429	.221
3	1	.571	.190
4	0.66	.762	.126
4.90	0	.933	0
5.25	-0.16	1	-.030
7	0	1.333	0

t = 15 min

x	y	x/ℓ	y/ℓ
0	0.40	0	.030
1	1	.074	.074
2	1.75	.148	.130
3	2.33	.222	.173
4	2.85	.296	.211
5	3.10	.370	.230
6	3.15	.444	.233
7	3.10	.519	.230
8	2.85	.593	.211
9	2.35	.667	.174
10	1.75	.741	.130
11	1	.815	.074
12.4	0	.919	0
13.5	-0.85	1	-.063
16	-0.55	1.185	-.041
18	-0.33	1.333	-.024

t = 60 min

x	y	x/ℓ	y/ℓ
0	0.50	0	.030
1	1.10	.060	.066
2	1.90	.119	.113
3	2.60	.179	.155
4	3.10	.239	.185
5	3.55	.299	.212
6	3.85	.358	.230
7.25	4.0	.433	.239
9	3.85	.537	.230
10	3.50	.597	.209
11	3	.657	.179
12	2.35	.716	.140
14	1.0	.836	.060
15.10	0	.901	0
16.75	-1.16	1	-.069
19	-0.75	1.134	-.045
21	-0.66	1.254	-.039
23	-0.60	1.373	-.036

t = 345 min

x	y	x/ℓ	y/ℓ
1	1.33	.052	.069
2	2.	.104	.104
3	2.66	.157	.139
4	3.30	.209	.172
5	3.85	.261	.201
6	4.16	.313	.217
7	4.40	.365	.230
8.50	4.55	.444	.237
10	4.33	.522	.226
12	3.75	.626	.196
14	2.50	.731	.130
16	1.0	.835	.052
17.40	0	.908	0
18	-0.45	.939	-.023
19.16	-1.20	1	-.063
20	-1.	1.044	-.052
22	-0.90	1.148	-.044
24	-0.80	1.253	-.042

Table 9

Summary of basic scour data

Fluid	Fluid specific weight (kg/m^3)	Sand diam. d (mm)	ζ_{max} (inch)	ℓ (inch)	ℓ' (inch)	U (cm/s)	$U^2/2g$ (inch)	U/w
Water	999	0.71	0.85	5.50	3.75	40	0.32	3.51
			1.60	11.25	7.00	60	0.72	5.26
	(63°F)	0.59	0.66	4.08	2.83	32	0.21	3.34
			1.38	8.83	5.63	48	0.46	5.02
			2.00	13.00	8.33	64	0.82	6.69
		0.42	0.97	6.60	4.25	39	0.31	5.80
			1.75	11.30	7.50	52	0.54	7.74
			3.83	22.60	15.60	78	1.22	11.61
Air	1.22	0.71	3.58	15.00	13.33	2020	820	4
			6.50	27.75	24.40	3030	1842	6
	(70°F)	0.59	0.72	4.80	4.80	900	163	2
			3.75	17.00	14.16	1800	650	4
			7.50	32.00	27.60	2700	1465	6
		0.42	2.27	9.95	9.00	1190	285	3.78
			4.55	19.16	17.40	1700	580	5.40
			9.44	40.50	33.50	2550	1307	8.10

APPENDIX C

LIST OF FIGURES

APPENDIX D

LIST OF TABLES

APPENDIX E

LIST OF PHOTOGRAPHS